

# Laboratory atomic transition data for precise optical quasar absorption spectroscopy

Michael T. Murphy,<sup>1\*</sup> Julian C. Berengut<sup>2</sup>

<sup>1</sup>Centre for Astrophysics and Supercomputing, Swinburne University of Technology, Hawthorn, Victoria 3122, Australia

<sup>2</sup>School of Physics, University of New South Wales, Sydney, NSW 2052, Australia

Accepted 2013 November 11. Received 2013 November 10; in original form 2013 October 30

## ABSTRACT

Quasar spectra reveal a rich array of important astrophysical information about galaxies which intersect the quasar line of sight. They also enable tests of the variability of fundamental constants over cosmological time and distance-scales. Key to these endeavours are the laboratory frequencies, isotopic and hyperfine structures of various metal-ion transitions. Here we review and synthesize the existing information about these quantities for 43 transitions which are important for measuring possible changes in the fine-structure constant,  $\alpha$ , using optical quasar spectra, i.e. those of Na, Mg, Al, Si, Ca, Cr, Mn, Fe, Ni and Zn. We also summarize the information currently missing that precludes more transitions being used. We present an up-to-date set of coefficients,  $q$ , which define the sensitivity of these transitions to variations in  $\alpha$ . New calculations of isotopic structures and  $q$  coefficients are performed for Si II and Ti II, including Si II  $\lambda$ 1808 and Ti II  $\lambda$ 1910.6/1910.9 for the first time. Finally, simulated absorption-line spectra are used to illustrate the systematic errors expected if the isotopic/hyperfine structures are omitted from profile fitting analyses.

To ensure transparency, repeatability and currency of the data and calculations, we supply a comprehensive database as Supporting Information. This will be updated as new measurements and calculations are performed.

**Key words:** atomic data – line: profiles – methods: laboratory: atomic – techniques: spectroscopic quasars: absorption lines – ultraviolet: general

## 1 INTRODUCTION

The absorption lines observed in the spectra of quasars have proved powerful probes of the high-redshift Universe. They offer the possibility for studying the interstellar, circumgalactic and intergalactic media along the quasar line of sight in considerable detail, regardless of the existence or brightness of any associated intervening galaxy (e.g. Schmidt 1963; Bahcall & Salpeter 1965; Gunn & Peterson 1965; Rauch 1998; Wolfe et al. 2005). Transitions from ionized metallic species, such as Si II, Mg II etc., are particularly useful because they can trace the kinematics of the intervening gas, i.e. the typical Doppler broadening of individual absorption features,  $b \lesssim 10 \text{ km s}^{-1}$ , is much narrower than the kinematic spread of gas in typical galaxies ( $\gtrsim 30 \text{ km s}^{-1}$ ), and their optical depths are sufficiently low that their damping wings do not swamp the detailed absorption profile (e.g. Lu et al. 1993; Churchill & Vogt 2001; Prochaska et al. 2008; Bouché et al. 2013). High-resolution optical spectroscopy of quasars also enables direct measurements of the column density of the absorbing ions which, together with that of the corresponding neutral hydrogen, provides accurate measures of the metallicity, dust-depletion and ionization characteris-

tics of the absorbing gas (e.g. Pettini et al. 1990; Prochaska & Wolfe 1996; Dessauges-Zavadsky et al. 2007). However, accurate laboratory data for these transitions are required for meaningful measurements to be made, particularly their rest-frame frequencies and oscillator strengths (e.g. Morton 1991, 2003).

The requirement for precise laboratory data is particularly acute when attempting to constrain changes in the fundamental constants of Nature using quasar absorption lines. The measured relative velocities of different metallic transitions in a quasar spectrum are directly proportional to deviations in the fine-structure constant,  $\alpha$ , between the absorbing cloud ( $\alpha_z$ ) and the current laboratory value ( $\alpha_0$ , Savedoff 1956; Dzuba et al. 1999b):

$$\Delta\alpha/\alpha \equiv \frac{\alpha_z - \alpha_0}{\alpha_0} \approx -\frac{\Delta v_i}{c} \frac{\omega_i}{2q_i}, \quad (1)$$

where the  $q$ -coefficient (defined in Appendix A) specifies the sensitivity of transition  $i$ 's frequency (or wavenumber,  $\omega_i$ ) to variations in  $\alpha$ , and  $c$  is the speed of light. Inaccuracies in the laboratory data for the metallic transitions used to measure  $\Delta\alpha/\alpha$  therefore translate to possible systematic errors in the analysis, potentially producing spurious detections of varying constants. Indeed, evidence has emerged for cosmological variations in  $\alpha$  from large samples of echelle quasar spectra with high resolving powers ( $R \gtrsim 45000$ ,

\* E-mail: mmurphy@swin.edu.au (MTM)

Webb et al. 1999; Murphy et al. 2001b; Webb et al. 2001; Murphy et al. 2003; Webb et al. 2011; King et al. 2012) which, so far, studies from smaller samples have neither confirmed or ruled out (e.g. Levshakov et al. 2006; Molaro et al. 2008, 2013). Furthermore, the first of these studies to use the ‘Many Multiplet method’ – the comparison of different transitions from different multiplets, often incorporating many ionic species – Webb et al. (1999), recognised that the accuracy of the previously-measured laboratory frequencies for the rest-frame ultraviolet (UV) transitions ( $\sim 2300\text{--}2800\text{ \AA}$ ) of Mg II and Fe II was a limiting factor in measuring  $\Delta\alpha/\alpha$  using quasar spectra. New laboratory measurements of the Mg II frequencies were conducted using Fourier Transform Spectrometers (FTSs) for that work (Pickering et al. 1998). It remains important that the laboratory data – especially rest-frame frequencies – for the transitions used in these studies are re-measured, scrutinized and refined.

An important step, particularly for varying- $\alpha$  studies, was recently made by Nave & Sansonetti (2011) and Nave (2012). By recalibrating the frequency scales of previous FTS measurements, they placed a large subset of the metal-ion transitions used so far for varying- $\alpha$  analyses onto a consistent frequency scale. They also showed that common scale to be consistent with the absolute frequencies of some transitions established using higher-precision, frequency comb techniques. It is therefore timely to review all the current metal-ion transitions used for varying- $\alpha$  studies and, where relevant and possible, to add further important information, such as isotopic and hyperfine structure measurements and calculations.

This paper reviews, compiles and synthesizes the extant measurements of rest-frame frequencies for the metal-ion transitions useful for measuring  $\Delta\alpha/\alpha$  in UV, optical and infrared quasar spectra. These are all electric dipole (E1) transitions from the ground state. We define “useful for measuring  $\Delta\alpha/\alpha$ ” to mean that the rest-frame frequency has been measured with velocity precision  $\delta v \lesssim 20\text{ m s}^{-1}$ , thereby ensuring that analysis of the quasar spectra should not be limited by the laboratory data. We consider here transitions of the following ions: Na I, Mg I and II, Al II and III, Si II and IV, Ca II, Cr II, Mn II, Fe II, Ni II and Zn II. Note that these are predominantly singly-ionized species, the dominant ionization state for these atoms in quasar absorbers with high enough column densities of hydrogen to be self-shielded from incoming ionizing UV photons. As such, these species might be expected to be largely inter-mixed within such absorbers and to occupy the same physical region.

The unresolved isotopic and hyperfine structures of the transitions of interest are also important to consider in varying- $\alpha$  analyses. The isotopic structures could be particularly important because we generally have no empirical estimates for the relative isotopic abundances prevailing in quasar absorption systems: if they differ from the terrestrial isotopic abundances, the absorption line centroids will differ slightly from that implied by the terrestrial ratios, potentially leading to systematic errors in  $\Delta\alpha/\alpha$  (Murphy et al. 2001a; Berengut et al. 2003; Ashenfelder et al. 2004). Theoretical models for the variations in the isotopic abundances in low metallicity environments were explored by Fenner et al. (2005), and show a wide variety of expected trends for different isotopes of different ionic species. However, to understand the impact of isotopic abundance variations on varying- $\alpha$  measurements, a more basic requirement is for the isotopic structures to be known from measurements, or at least estimated from theory. This paper presents calculations of the frequencies of the isotopic and hyperfine components of the transitions of interest and highlights cases of significant uncertainty.

Finally, this paper provides a self-consistent set of recommended sensitivity coefficients,  $q$ , for these metal-ion transitions. Following Dzuba et al. (1999b), the  $q$ -coefficients have been calculated with a variety of methods by several authors, all showing good consistency. It is important to realise that errors in the calculated  $q$  coefficients cannot produce spuriously non-zero measurements of  $\Delta\alpha/\alpha$ ; only systematic errors which introduce measured velocity shifts between transitions can do that – see equation (1). Nevertheless, detailed comparison of any non-zero measurements of  $\Delta\alpha/\alpha$  by different groups is facilitated by a consistent set of  $q$  coefficients.

This paper is organised as follows. In Section 2 we tabulate the laboratory atomic data for the transitions of interest. We summarise the existing measurements and also fully describe our calculations, where required, to connect the measured quantities with the frequencies, isotopic and/or hyperfine structures recommended for analysis of quasar absorption spectra. Section 3 describes the systematic effects on measured quantities in quasar absorption analyses (redshifts, column densities and Doppler broadening parameters) if the isotopic and hyperfine structures of these transitions are ignored when analysing quasar spectra. In Section 4 we summarize the important laboratory transition information still missing for the ions considered in this paper and conclude. An appendix describes our new calculations of the  $q$ -coefficients and isotopic structures for transitions of Si II and Ti II.

## 2 ATOMIC DATA

Tables 1–11 provide the important laboratory data for quasar absorption line analysis, focussing particularly on the frequencies recommended for constraining cosmological changes in  $\alpha$ . The isotopic and hyperfine structures are illustrated in Figs. 1–10 where measurements or calculations were available or newly performed. The structure of these tables and figures is described in Section 2.1.

Section 2.2 describes the general basis for our calculations of composite, isotopic and hyperfine frequencies. For each atom, a subsequent subsection (Sections 2.3–2.13) describes the laboratory frequency measurements and the composite, isotopic and/or hyperfine frequency calculations in detail. To establish the relative reliability of different transitions for varying- $\alpha$  analyses, particular attention is paid to whether each transition has been reproduced in more than one experiment and how its frequency has been calibrated. For the latter, of particular note is whether the original FTS measurements were calibrated with the Ar II transition frequencies of Norlén (1973) or those of Whaling et al. (1995). Nave & Sansonetti (2011) and Nave (2012) determined reliable conversion factors between these two calibration scales, with the Whaling et al. scale being consistent with more precise, absolute frequency measurements using frequency combs. Therefore, all frequencies quoted in Tables 1–11 are either on the absolute (frequency comb) or Whaling et al. frequency scales, with conversions from Norlén calibrations described in Sections 2.3–2.13 where necessary.

To ensure the accuracy and transparency of all the information provided in Tables 1–11 and calculations described in Sections 2.2 and 2.3–2.13, we also provide a comprehensive ‘Atomic Data spreadsheet’ in the online Supporting Information. This allows future incorporation of new/alternative measurements and/or calculations.

## 2.1 Data tables and isotopic/hyperfine structure figures

In Tables 1–11 the transitions are named by truncating their vacuum wavelengths to the nearest Ångström according to the usual convention in quasar absorption work. They are further identified by their lower and upper state electronic configurations, and “ID” labels. The latter act as a ‘short-hand’ notation to assist specifying a set of transitions analysed in a particular absorption system (e.g. Murphy et al. 2001a; King et al. 2012). The ID’s superscript is the ionization stage and its subscript is the transition’s rank among those falling redwards of H I Lyman- $\alpha$  for that ion in order of decreasing oscillator strength. Hyperfine components are also identified by the quantum number,  $F$ , which represents the vector sum of the nuclear and electron angular momenta. The relative atomic mass,  $A$ , is provided for each ion; these determine the relative widths of quasar absorption lines from different metallic species when the gas is dominated by thermal broadening. The mass number identifies individual isotopic or hyperfine components under the same “A” column. Rows pertaining to isotopic and hyperfine components are shown in italics. The tables also provide the relevant ionization potentials for each ion, i.e. the energy required to create the ion from the next lowest ionization stage (IP<sup>-</sup>) and that required to reach the next stage (IP<sup>+</sup>).

The laboratory frequency,  $f_0$ , is given as the wavenumber,  $\omega_0$ , in the tables:  $\omega_0 \equiv f_0/c = 1/\lambda_0$  for  $\lambda_0$  the wavelength in vacuum. For convenience, the tables also provide  $\lambda_0$  for each transition (converted from the measured frequency). For some transitions, individual isotopic and/or hyperfine structure wavenumbers were measured in the laboratory experiments. For others, only the (relative) splitting between isotopic/hyperfine components was measured or, more often, only calculated, and the centroid of the ‘composite’ transition – the weighted sum of its components – was measured. Our approach for inferring the unmeasured quantities in these cases is described below in Section 2.2, and the details for each transition are given in Sections 2.3–2.13. To summarize that information in Tables 1–11, we provide a flag,  $X$ , defined as follows:

$$X = \begin{cases} 0 & \text{Measured frequency;} \\ 1 & \text{Inferred from component frequencies;} \\ 2 & \text{Inferred from measured composite frequency and} \\ & \text{measured component splitting;} \\ 3 & \text{Inferred from measured composite frequency and} \\ & \text{calculated component splitting;} \\ 4 & \text{Inferred from measured component frequency and} \\ & \text{measured component splitting;} \\ 5 & \text{Inferred from measured component frequency and} \\ & \text{calculated component splitting.} \end{cases} \quad (2)$$

The variety and challenges of UV FTS laboratory experiments, plus the significant improvement in precision and accuracy offered by frequency comb techniques, result in a wide range of frequency uncertainties for different transitions and their isotopic/hyperfine components. For convenience in quasar absorption-line work, and particularly for varying- $\alpha$  analyses, Tables 1–11 present these uncertainties in velocity space,  $\delta v$ . These range from just  $0.04 \text{ m s}^{-1}$  for the frequency comb-calibrated Mg II isotopes (see Table 2), up to  $\approx 20 \text{ m s}^{-1}$  for the Ni II transitions (see Table 10), the maximum measurement uncertainty allowed under our definition of “useful for  $\Delta\alpha/\alpha$ ”.

An important parameter for accurate modelling of quasar absorption lines is the oscillator strength of each transition,  $f$ . The values provided in Tables 1–11 are those compiled by Morton (2003). For isotopic components, the relative terrestrial isotopic

abundance from Rosman & Taylor (1998) is presented as a percentage. This fraction is further broken down for hyperfine components according to the relative level populations expected under the assumption of local thermodynamic equilibrium (LTE). For the relevant transitions discussed in this paper – those of  $^{23}\text{Na I}$ ,  $^{25}\text{Mg II}$ ,  $^{27}\text{Al III}$ ,  $^{43}\text{Ca II}$ ,  $^{55}\text{Mn II}$  and  $^{67}\text{Zn II}$  – photo-excitation from the cosmic microwave background is sufficient to make this a very good approximation<sup>1</sup>.

Finally, the tables also provide the recommended  $q$  coefficient for each transition, i.e. its sensitivity to variations in  $\alpha$ . For single-valence-electron ions (i.e. Na I, Mg II, Al III, Si IV, and Ca II) our recommended  $q$  coefficients were calculated by Dzuba & Johnson (2007) using the all-order coupled-cluster single-double method with added third-order many-body perturbation theory (MBPT) and Breit corrections. Note that the quoted uncertainties are not statistical and should not be considered or used as such. Instead, the errors quoted are indicative of the (small) discrepancy with other methods: second-order MBPT (Dzuba et al. 1999a), second-order Brueckner orbitals (Berengut et al. 2004), or second-order MBPT with Breit corrections (Savukov & Dzuba 2008). Note that Breit corrections to the  $q$  coefficients are very small in all the transitions considered. For all the many-valence-electron ions, at a minimum the  $q$  coefficients are calculated using configuration interaction (CI). In many cases, we present results obtained using the atomic structure package AMBiT, an implementation of the combination of CI and MBPT described in Berengut et al. (2006) (see also Dzuba et al. 1996; Berengut et al. 2005). More details of this method are presented in Appendix A where we also present new calculations for the transitions of Si II and Ti II shown in Tables 4 and 6, respectively. References for the origin of the other many-valence-electron ions are given in the relevant subsection for each ion, but in all cases the results we present in this work show a high level of consistency across methods and authors.

Figures 1–10 illustrate the isotopic and/or hyperfine structures for the transitions studied here, where available. Each panel of each Figure depicts a single transition, with the black vertical lines indicating the velocity-space positions and relative strengths (‘intensities’) of the individual components from Tables 1–11. The velocity zero point (vertical cyan line) corresponds to the composite wavelength of the transition. The ID letter for each transition is provided in the top right-hand corner of its panel and the components are labelled by their mass number,  $A$ . The blue curve in each panel represents the sum of Gaussian functions centred on, and with the relative amplitudes of, the isotopic/hyperfine components. The Gaussian width is set to a full-width-at-half-maximum (FWHM) of  $0.3 \text{ km s}^{-1}$ , equivalent to a resolving power of  $R = 1 \times 10^6$ , for all components in all the Figures. This aids the eye in quickly determining how important the isotopic/hyperfine structure is for any given transition (assuming terrestrial isotopic abundances and LTE hyperfine level populations). For example, one can immediately see that the isotopic structure of the Mg transitions (Fig. 2) could be important for correctly modelling quasar absorption lines, whereas it will be less important for the Fe II transitions (Fig. 9), assuming that, for the latter, the theoretical estimates of the isotopic structure are approximately correct.

<sup>1</sup> The largest ground-state hyperfine energy splitting considered in this paper is  $8 \times 10^{-5} \text{ eV}$  for  $^{55}\text{Mn II } \lambda 2606$ . This is an order of magnitude smaller than the present-day cosmic microwave background photon energy of  $\approx 7 \times 10^{-4} \text{ eV}$ , so we can expect all hyperfine levels in the ground state to be equally populated at all redshifts.

## 2.2 Composite, isotopic and hyperfine frequency calculations

With few exceptions, the transitions in Tables 1–11 generally comprise multiple isotopic and/or hyperfine components. At the resolving powers used in most quasar absorption line work ( $R \lesssim 100000$ ), and given the typical Doppler broadening prevailing in most quasar absorption clouds ( $b \sim 1\text{--}10 \text{ km s}^{-1}$ ), this multi-component structure is not important to model in most studies. However, Section 3.2 below demonstrates that care must be taken when modelling Al III and Mn II absorption profiles because their hyperfine structures are particularly broad and can significantly affect column density and Doppler broadening estimates. For varying- $\alpha$  work, the velocity centroid of an absorption line is the key measurement, so modelling the unresolved structure of each transition can be very important. This is demonstrated explicitly in Section 3.1.

Unfortunately, laboratory measurements with sufficient resolution and suppression of Doppler broadening to resolve apart the isotopic/hyperfine components of these transitions are few. Thus, direct measurements of their isotopic/hyperfine component frequencies, or even the relative splittings, are not available. However, in many cases the splittings have been calculated, or can be derived from other measured quantities with sufficient accuracy. In these cases, we define the relationship between the composite and component wavenumbers as

$$\omega_{\text{comp}} = \sum_i^N a_i \omega_i, \quad (3)$$

where the coefficient  $a_i$  is the relative isotopic abundance of the  $i$ th component multiplied by its relative hyperfine intensity, normalized such that  $\sum_i^N a_i = 1$  over the  $N$  components. If, as is most usual, the composite wavenumber has been measured and the isotopic and/or hyperfine component separations,  $\Delta\omega_i \equiv \omega_j - \omega_i$ , are known, or can be estimated, then the wavenumber for the  $j$ th component is calculated as

$$\omega_j = a_j^{-1} \left( \omega_{\text{comp}} - \sum_{i \neq j}^N a_i \Delta\omega_i \right). \quad (4)$$

For calculating isotopic structures, the frequency shift,  $\delta\nu^{A',A} \equiv \nu^{A'} - \nu^A$ , for a given transition in an isotope with mass number  $A'$  relative to the same transition in one with mass number  $A$ , may be expressed as (e.g. Berengut et al. 2003)

$$\delta\nu^{A',A} = (k_{\text{NMS}} + k_{\text{SMS}}) \left( \frac{1}{A'} - \frac{1}{A} \right) + F_{\text{FS}} \delta\langle r^2 \rangle^{A',A}, \quad (5)$$

where  $k_{\text{NMS}} \equiv -\nu^A m_e$  is the normal mass shift constant with  $m_e$  the electron mass in atomic mass units,  $k_{\text{SMS}}$  is the specific mass shift constant,  $F_{\text{FS}}$  is the field shift constant and  $\delta\langle r^2 \rangle^{A',A}$  is the difference between the root-mean-square nuclear charge radii of the two isotopes. In Appendix A we detail new calculations of  $k_{\text{SMS}}$  and  $F_{\text{FS}}$  for the Si II and Ti II transitions shown in Tables 4 and 6 respectively. Previously published values for  $k_{\text{SMS}}$  and  $F_{\text{FS}}$  are used to calculate isotopic structures using equation (5) for some transitions of Mg II, Fe II and Zn II in Sections 2.4, 2.11 and 2.13 respectively.

The hyperfine energy shift for given nuclear and electron states can be expressed, to second order, as (e.g. Sur et al. 2005)

$$\Delta E_{\text{hyp}} = \Delta E_{\text{M1}} + \Delta E_{\text{E2}}, \quad (6)$$

where the magnetic dipole and electric quadrupole terms are, respectively,

$$\Delta E_{\text{M1}} = \frac{A}{2} K \quad \text{and} \quad \Delta E_{\text{E2}} = \frac{B}{2} C, \quad (7)$$

where  $A$  and  $B$  are the magnetic dipole and electric quadrupole hyperfine constants, respectively, with

$$K \equiv F(F+1) - I(I+1) - J(J+1) \quad (8)$$

and

$$C \equiv \frac{3K(K+1) - 4I(I+1)J(J+1)}{2I(2I-1)2J(2J-1)}. \quad (9)$$

Here,  $I$ ,  $J$  and  $F$  are the quantum numbers representing the total angular momentum of the nuclear state,  $I$ , the electron ground state,  $J$ , and their vector sum,  $F$ . The relative probabilities for the transitions to the excited state hyperfine levels, defined by the electron and total angular momenta,  $J'$  and  $F'$ , is given by the product of the level degeneracies and the Wigner  $6J$ -symbol,

$$S = (2F+1)(2F'+1) \begin{Bmatrix} J & F & I \\ F' & J' & 1 \end{Bmatrix}^2. \quad (10)$$

Hyperfine structures are calculated using equations (6)–(10) with previously measured or calculated values of  $A$  and  $B$  for transitions of  $^{23}\text{Na I}$ ,  $^{25}\text{Mg II}$ ,  $^{43}\text{Ca II}$  and  $^{67}\text{Zn II}$  in Sections 2.3, 2.4, 2.7 and 2.13 respectively. In those cases, and for the measured hyperfine structures of  $^{27}\text{Al III}$  and  $^{55}\text{Mn II}$ , the splitting of the excited states is found to be negligibly small, so only the hyperfine structure of the ground states is important to consider for quasar absorption line studies. This is discussed further in the relevant sections below and explicitly reflected in Tables 1, 2, 3, 5, 8 and 11. We have not derived the hyperfine structure for other isotopic species with odd nucleon numbers ( $^{29}\text{Si II}$ ,  $^{47,49}\text{Ti II}$ ,  $^{53}\text{Cr II}$ ,  $^{57}\text{Fe II}$ ), either because the relevant measurements/estimates of  $A$  and  $B$  are not available in the literature, or their magnetic moments are relatively small, leading us to expect small values for  $A$  and  $B$ .

All calculations of composite, isotopic and hyperfine component wavenumbers are presented in detail, and can be trivially modified to accommodate new or changed information, in the comprehensive ‘Atomic Data spreadsheet’ in the online Supporting Information.

## 2.3 Sodium

Table 1 provides the atomic data for the two strongest Na I transitions which are common, though often not particularly strong, in quasar absorption systems. Figure 1 illustrates the hyperfine structures for these transitions. The Na I  $\lambda\lambda 5891/5897$  doublet, or D2 and D1 transitions are observable at redshifts  $z \lesssim 0.6$  in optical quasar absorption spectra. However, they have not been used so far in varying- $\alpha$  studies (to our knowledge) for three main reasons: (i) they are typically much weaker than the ubiquitous Mg and Fe II transitions observable at the same redshifts; (ii) they often fall in spectral regions containing significant telluric absorption; and (iii) their frequencies are relatively insensitive to variations in  $\alpha$ . Nevertheless, being the strongest Na I transitions from the ground state by a factor of  $\gtrsim 30$  (Morton 2003), they are the only Na I transitions that are suitable for varying- $\alpha$  work. Na has only one stable isotope ( $^{23}\text{Na}$ ), so it is immune to systematic effects in varying- $\alpha$  analyses related to isotopic abundance evolution (along with Al and Mn). However, the D1/D2 lines do have hyperfine structure, which is dominated by the  $\sim 1 \text{ km s}^{-1}$  splitting of the ground state, and these have been measured to high precision (see below).

To our knowledge, the most recent and most precise absolute frequency measurements for the Na I D lines are those of Juncar et al. (1981). Using a saturated-absorption technique, they locked a tunable dye laser to well-studied hyperfine components of iodine

**Table 1.** Laboratory data for transitions of Na of interest for quasar absorption-line varying- $\alpha$  studies described in Section 2.3. See Section 2.1 for full descriptions of each column.

Ion	Tran.	$A$	$\omega_0$ [ $\text{cm}^{-1}$ ]	$X$	$\lambda_0$ [ $\text{\AA}$ ]	$\delta\nu$ [ $\text{m s}^{-1}$ ]	Lower state	Upper state	ID	IP <sup>-</sup> , IP <sup>+</sup> [eV]	$f$ or %	$q$ [ $\text{cm}^{-1}$ ]
Na I	5891	22.9898	16973.366206(43)	1	5891.583248(15)	0.76	$3s\ ^2S_{1/2}$	$3p\ ^2P_{3/2}^o$	Na <sub>1</sub>	—, 5.14	0.6408	$62^a(2)$
		23	16973.401853 <sup>b,c,d</sup>	4	5891.570875		$F = 1$	$F = 0, 1, 2$			37.5%	
		23	16973.344818 <sup>b,c,d</sup>	4	5891.590672		$F = 2$	$F = 1, 2, 3$			62.5%	
	5897	22.9898	16956.170247(43)	1	5897.558148(15)	0.76		$3p\ ^2P_{1/2}^o$	Na <sub>2</sub>		0.3201	$45^a(2)$
	23	16956.208494 <sup>c,e,d</sup>	4	5897.544845		$F = 1$	$F = 1, 2$			37.5%		
	23	16956.147299 <sup>c,e,d</sup>	4	5897.566130		$F = 2$	$F = 1, 2$			62.5%		

References: <sup>a</sup>Dzuba & Johnson (2007); <sup>b</sup>Beckmann et al. (1974); <sup>c</sup>Juncar et al. (1981); <sup>d</sup>Yei et al. (1993); <sup>e</sup>van Wijngaarden & Li (1994).

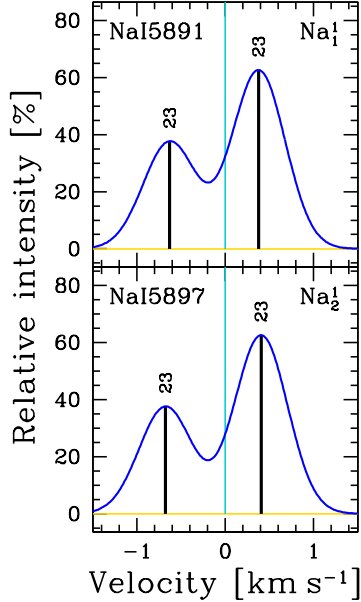


**Figure 1.** Na transition hyperfine structures in Table 1 described in Section 2.3. See Section 2.1 for Figure details.

gas ( $I_2$ ) transitions near the ‘cross-over’ (i.e. average) frequencies of particular hyperfine components of the Na I transitions. Within the final measurement uncertainties they present, their  $I_2$  calibration scale is consistent with modern frequency comb-calibrated measurements of the same  $I_2$  reference lines (e.g. Balling & Kr̄en 2008), so we have not corrected their Na I frequency measurements for calibration differences.

Starting from the basic ‘cross-over’ frequency measurements of Juncar et al. (1981), we used modern measurements of the ground and excited state hyperfine splittings to determine absolute frequencies for all hyperfine components. The magnetic dipole hyperfine constant ( $A$ ) for the ground state was taken from Beckmann et al. (1974) while those for the D1 and D2 excited states were taken from van Wijngaarden & Li (1994) and Yei et al. (1993), respectively. The electric quadrupole hyperfine constant ( $B$ ) for the D2 line was also taken from the latter. The hyperfine structure was then determined via equations (6)–(10). In Table 1 we average over the hyperfine splitting of the excited states because it is negligible ( $\sim 60\text{ m s}^{-1}$ ) compared to the large ground-state splitting ( $\sim 1\text{ km s}^{-1}$ ). Finally, the composite frequencies were determined from the hyperfine component frequencies via equation (3). We note that the composite wavelengths in Table 1 differ slightly (up to  $1.1\sigma$ , i.e.  $1.5 \times 10^{-5}\text{ \AA}$ , or  $0.8\text{ m s}^{-1}$ ) from those reported by Juncar

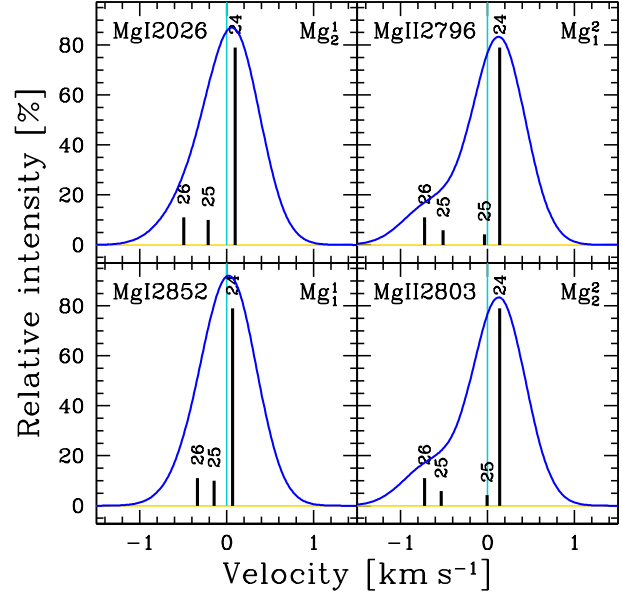


**Figure 2.** Mg transition isotopic and hyperfine structures in Table 2 described in Section 2.4. See Section 2.1 for Figure details.

et al. (1981), a difference we suspect is attributable to the updated excited-state hyperfine structures we employed.

The final hyperfine splittings of the Na I D lines illustrated in Fig. 1 are relatively broad ( $\sim 1\text{ km s}^{-1}$ ) and render the final line shapes significantly asymmetric. Therefore, absorption line modelling of modern, high-resolution quasar spectra, could be inaccurate if the hyperfine isotopic structure is not taken into account. This is considered further in Section 3.

## 2.4 Magnesium

Table 2 provides the atomic data for the two strongest Mg I transitions and the Mg II doublet which is very prominent in quasar absorption systems. Figure 2 illustrates the isotopic and hyperfine structures for these transitions. Mg I  $\lambda 2852$  is the strongest Mg I transition by more than an order of magnitude and is commonly observed, while Mg I  $\lambda 2026$  is often blended with the Zn II  $\lambda 2026$  transition  $50\text{ km s}^{-1}$  bluewards of it and, typically, of similar optical depth. The Mg II  $\lambda\lambda 2796/2803$  doublet is one of the strongest and, therefore, easily-identifiable metallic features of quasar absorbers. The ubiquity of Mg II  $\lambda\lambda 2796/2803$  in quasar spectra make these transitions prominent in varying- $\alpha$  studies. Only two other Mg II transitions fall redwards of the Lyman- $\alpha$  forest, the  $\lambda\lambda 1239/1240$

**Table 2.** Laboratory data for transitions of Mg of interest for quasar absorption-line varying- $\alpha$  studies described in Section 2.4. See Section 2.1 for full descriptions of each column.

Ion	Tran.	A	$\omega_0$ [cm <sup>-1</sup> ]	X	$\lambda_0$ [Å]	$\delta\nu$ [m s <sup>-1</sup> ]	Lower state	Upper state	ID	IP <sup>-</sup> , IP <sup>+</sup> [eV]	f or %	q [cm <sup>-1</sup> ]
Mg I	2026	24.3050	49346.772620(36)	1	2026.4749788(15)	0.2	3s <sup>2</sup> 1S <sub>0</sub>	3s4p 1P <sub>1</sub> <sup>o</sup>	Mg <sub>2</sub> <sup>1</sup>	—, 7.65	0.113	87 <sup>a,b</sup> (7)
		26	49346.854173(40) <sup>c</sup>	0	2026.4716298(16)	0.2					11.01%	
		25	49346.807724(40) <sup>c</sup>	0	2026.4735372(16)	0.2					10.00%	
		24	49346.756809(35) <sup>c</sup>	0	2026.4756281(14)	0.2					78.99%	
	2852	24.3050	35051.28076(19)	1	2852.962797(15)	1.6		3s3p 1P <sub>1</sub> <sup>o</sup>	Mg <sub>1</sub> <sup>1</sup>		1.83	90 <sup>a,b</sup> (10)
		26	35051.32015(25) <sup>d</sup>	0	2852.959591(20)	2.1					11.01%	
		25	35051.29784(25) <sup>d</sup>	0	2852.961407(20)	2.1					10.00%	
		24	35051.27311(17) <sup>d</sup>	0	2852.963420(14)	1.5					78.99%	
Mg II	2796	24.3050	35760.85414(20)	1	2796.353790(16)	1.7	3s 2S <sub>1/2</sub>	3p 2P <sub>3/2</sub> <sup>o</sup>	Mg <sub>1</sub> <sup>2</sup>	7.65, 15.04	0.6155	212 <sup>e</sup> (2)
		26	35760.9403866(53) <sup>f</sup>	0	2796.34704565(42)	0.04					11.01%	
		25	35760.85850(64) <sup>f,g,h</sup>	3	2796.353449(50)	5.4	F = 2	F = 1, 2, 3			4.17%	
		25	35760.91502(64) <sup>f,g,h</sup>	3	2796.349030(50)	5.4	F = 3	F = 2, 3, 4			5.83%	
	2803	24.3050	35669.30440(20)	1	2803.530982(16)	1.7		3p 2P <sub>1/2</sub> <sup>o</sup>	Mg <sub>2</sub> <sup>2</sup>		0.3058	121 <sup>e</sup> (2)
		26	35669.3905712(53) <sup>f</sup>	0	2803.52420938(42)	0.04					11.01%	
		25	35669.30492(64) <sup>f,g,h</sup>	3	2803.530941(50)	5.4	F = 2	F = 2, 3			4.17%	
		25	35669.36798(64) <sup>f,g,h</sup>	3	2803.525985(50)	5.4	F = 3	F = 2, 3			5.83%	
		24	35669.2876697(53) <sup>f</sup>	0	2803.53229720(42)	0.04					78.99%	

References: <sup>a</sup>Berengut et al. (2005); <sup>b</sup>Savukov & Dzuba (2008); <sup>c</sup>Hannemann et al. (2006); <sup>d</sup>Salumbides et al. (2006); <sup>e</sup>Dzuba & Johnson (2007); <sup>f</sup>Batteiger et al. (2009); <sup>g</sup>Itano & Wineland (1981); <sup>h</sup>Sur et al. (2005).

doublet, and these are 3 orders of magnitude weaker (Morton 2003), so they are not usually suitable for varying- $\alpha$  studies.

For Mg I, Hannemann et al. (2006) and Salumbides et al. (2006) measured the frequencies of the 24, 25 and 26 isotopic components of the  $\lambda$ 2026 and  $\lambda$ 2852 transitions, respectively, using laser frequency comb techniques. The frequencies are therefore on an absolute scale and the uncertainties are very small, corresponding to velocity uncertainties of  $\sim 0.2$  m s<sup>-1</sup> for the  $\lambda$ 2026 transition and  $\sim 2$  m s<sup>-1</sup> for  $\lambda$ 2852. The hyperfine structure of the 25 isotope was not resolved in the measurements of either transition; for  $\lambda$ 2026 the separation between the <sup>25</sup>Mg I hyperfine components is just  $\sim 20$  Hz, or  $\sim 4$  m s<sup>-1</sup>. Therefore, we do not represent the <sup>25</sup>Mg I hyperfine structure in Table 2. The composite wavelengths for the two Mg I transitions were calculated according to equation (3).

The absolute frequencies of the 24 and 26 isotopic components of the Mg II  $\lambda\lambda$ 2796/2803 doublet have also been measured with high precision using frequency comb techniques by Batteiger et al. (2009). Their uncertainties correspond to just  $\sim 4$  cm s<sup>-1</sup>. However, the transitions of the 25 isotope could not be produced in this experiment. Instead, Batteiger et al. (2009) used equation (5) to calculate the <sup>25,24</sup>Mg II isotope shifts, drawing on calculations of the field shift constants ( $F_{FS}$ ) from Safronova & Johnson (2001), Berengut et al. (2003) and Tupitsyn et al. (2003) and the nuclear charge radii ( $\delta\langle r^2 \rangle^{25,24}$ ) measurements of Angeli (2004), finding  $\delta\nu^{25,24} = 1621$  and 1620 MHz for the  $\lambda$ 2796 and  $\lambda$ 2803 transitions, respectively. The uncertainty of 19 MHz in each of these estimates, which is dominated by the measurement uncertainty in  $\delta\langle r^2 \rangle^{25,24}$ , ultimately limits the precision of the 25 isotope and also composite frequencies quoted in Table 2.

To calculate the hyperfine splitting in the <sup>25</sup>Mg II  $\lambda\lambda$ 2796/2803 transitions we used equations (6)–(10) with the magnetic dipole hyperfine constants ( $A$ ) measured for the ground state by Itano & Wineland (1981) and calculated for the excited states by Sur et al. (2005); we also use Sur et al. (2005)’s calculated electric quadrupole hyperfine constant ( $B$ ). Mg has a nuclear spin of  $I = 5/2$  so that the <sup>25</sup>Mg II  $\lambda$ 2796 ( $\lambda$ 2803) transition has 6 (4) allowed transitions, three (two) from each of the two ground states

( $F = 2$  and 3). The hyperfine splitting is dominated by that in the ground states, which is itself less than a tenth of the <sup>26,24</sup>Mg II isotopic splitting in these transitions. Therefore, as illustrated in Fig. 2, we represent the <sup>25</sup>Mg II  $\lambda\lambda$ 2796/2803 hyperfine structures with just two components each. All details of these calculations are provided in the online Supporting Information.

The isotopic structures for the Mg transitions, particularly those of Mg II, illustrated in Fig. 2 are notably broad and asymmetric, with the 24–26 isotopic component separation being up to  $\sim 0.85$  km s<sup>-1</sup> and with the lightest isotope (<sup>24</sup>Mg) being the most abundant. These facts, combined with the ubiquity of the Mg II  $\lambda\lambda$ 2796/2803 doublet, imply that absorption line modelling could be inaccurate if the isotopic structure is not taken into account or the relative Mg isotopic abundances in quasar absorbers are significantly different to those in the terrestrial environment. This was recognised as a potential source of significant errors for varying- $\alpha$  studies by Webb et al. (1999) and Murphy et al. (2001b,a) (see also, e.g., Murphy et al. 2003; Ashenfelder et al. 2004; Fenner et al. 2005).

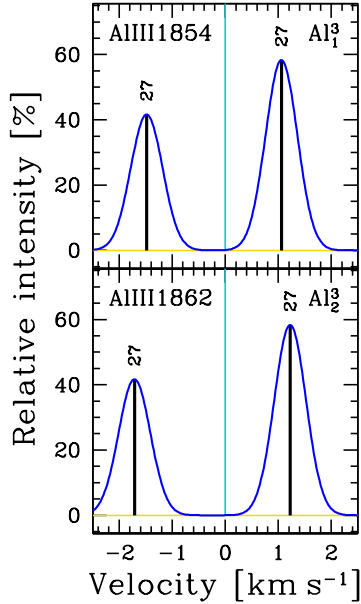
The  $q$  coefficients for Mg I, a two-valence-electron atom, have been calculated with the same CI+MBPT method described in Appendix A by (Berengut et al. 2005) and by a different implementation that includes the Breit interaction by Savukov & Dzuba (2008). The values recommended in Table 2 for Mg I are the simple average from these two works. The errors quoted for these  $q$  coefficients reflect the differences between these results, which are largely due to the Breit interaction.

## 2.5 Aluminium

Table 3 provides the atomic data for the single strong Al II transition and the Al III doublet. Figure 3 illustrates the hyperfine structures for the latter. Al II  $\lambda$ 1670 is one of only 3 transitions of Al II known in the UV and it is the strongest by almost a factor a 1000 (Morton 2003). It is an important ‘‘anchor’’ line for many-multiplet studies of  $\alpha$  variation: it is a strong transition from a relatively abundant ion, so it is detected even in low column-density absorbers, and it

**Table 3.** Laboratory data for transitions of Al of interest for quasar absorption-line varying- $\alpha$  studies described in Section 2.5. See Section 2.1 for full descriptions of each column.

Ion	Tran.	$A$	$\omega_0$ [cm <sup>-1</sup> ]	$X$	$\lambda_0$ [Å]	$\delta\nu$ [m s <sup>-1</sup> ]	Lower state	Upper state	ID	IP <sup>-</sup> , IP <sup>+</sup> [eV]	$f$ or %	$q$ [cm <sup>-1</sup> ]
Al II	1670	26.9815	59851.976(4) <sup>a</sup>	0	1670.78861(11)	20.0	3s <sup>2</sup> 1S <sub>0</sub>	3s3p 1P <sub>1</sub> <sup>o</sup>	Al <sub>1</sub> <sup>2</sup>	5.99, 18.83	1.74	270 <sup>b,c</sup> (10)
Al III	1854	26.9815	53916.5480(11)	1	1854.718146(39)	6.3	3s 2S <sub>1/2</sub>	3p 2P <sub>3/2</sub> <sup>o</sup>	Al <sub>1</sub> <sup>3</sup>	18.83, 28.45	0.559	458 <sup>d</sup> (6)
		27	53916.8149(8) <sup>a</sup>	0	1854.708966(28)	4.4	$F = 2$	$F = 1, 2, 3$			41.67%	
	27	53916.3574(8) <sup>a</sup>	0	1854.724704(28)	4.4	$F = 3$	$F = 2, 3, 4$			58.33%		
	1862	26.9815	53682.8884(11)	1	1862.790974(39)	6.3		3p 2P <sub>1/2</sub> <sup>o</sup>	Al <sub>2</sub> <sup>3</sup>		0.278	224 <sup>d</sup> (8)
	27	53683.1953(8) <sup>a</sup>	0	1862.780325(28)	4.5	$F = 2$	$F = 2, 3$			41.67%		
	27	53682.6692(8) <sup>a</sup>	0	1862.798581(28)	4.5	$F = 3$	$F = 2, 3$			58.33%		

References: <sup>a</sup>Griesmann & Kling (2000); <sup>b</sup>Angstmann et al. (2004); <sup>c</sup>Savukov & Dzuba (2008); <sup>d</sup>Dzuba & Johnson (2007).**Figure 3.** Al transition hyperfine structures in Table 3 described in Section 2.5. See Section 2.1 for Figure details.

has a very low sensitivity to  $\alpha$  variation (i.e. a small  $q$ -coefficient). Si II  $\lambda 1526$  is the only similar case in the far UV (i.e. observed at high redshift). The Al III  $\lambda\lambda 1854/1862$  doublet comprises the only known UV transitions of Al III (Morton 2003) but it is commonly observed in quasar absorbers despite Al II being the dominant ion in self-shielded gas. One concern for varying- $\alpha$  studies is whether the Al II and Al III absorption profiles are expected to trace the same velocity structures, i.e. whether the doubly-ionised transitions can be analysed together with singly-ionised transitions in the many-multiplet method. However, the empirical evidence so far suggests no systematic problem in this regard (e.g. Murphy et al. 2001b). Importantly, Al has only one stable isotope (<sup>27</sup>Al), making it one of only three elements discussed in this paper which is immune to systematic effects in varying- $\alpha$  analyses related to isotopic abundance evolution (the others being Na and Mn).

The Al II  $\lambda 1670$  laboratory wavenumber has been measured with 20 m s<sup>-1</sup> precision by Griesmann & Kling (2000) using a FTS and Penning discharge lamp. Although <sup>27</sup>Al has a relatively large magnetic dipole moment ( $\mu = +3.6$  nuclear magnetons), no hyperfine structure was resolved by Griesmann & Kling for the spin-zero Al II  $\lambda 1670$  transition. The wavenumber was calibrated using the Ar II scale of Whaling et al. (1995), placing it, in principle, on the same calibration scale as the other transitions in this paper (i.e. that

of Nave 2012). We are not aware of any similarly-precise measurements of Al II  $\lambda 1670$ .

The wavenumbers for the hyperfine components of Al III  $\lambda\lambda 1854/1862$  were measured using a FTS and hollow cathode lamp (HCL) by Griesmann & Kling (2000). With a nuclear spin of  $I = 5/2$ , 6 hyperfine components are expected in each transition, i.e. 3 from each of the two ground states ( $F = 2$  and 3). Only the ground state hyperfine structures were resolved by Griesmann & Kling so we average over any splitting in the excited states and represent each of the Al III  $\lambda\lambda 1854/1862$  transitions by two hyperfine components in Table 3 and Fig. 3. For consistency with transitions of other ions considered here, composite wavelengths are also presented in Table 3, derived from the measured hyperfine wavenumbers using equation (4). However, as illustrated in Fig. 3, the hyperfine structure is very widely-spaced –  $>2.5$  km s<sup>-1</sup> – so, for interpreting high-resolution ( $R \gtrsim 30000$ , or FWHM  $\lesssim 10$  km s<sup>-1</sup>) quasar absorption spectra, we recommend using the individual hyperfine components, not treating them as a single, composite line. Indeed, section 3 shows that the effects of ignoring this hyperfine structure in quasar absorption studies are relatively large. Like Al II  $\lambda 1670$ , the Al III wavenumbers measured by Griesmann & Kling were placed on the Whaling et al. (1995) calibration scale and have not, to our knowledge, been reproduced to similar precision in subsequent experiments.

The  $q$  coefficients for Al II, a two-valence-electron ion, have been calculated using a CI+MBPT method, similar to that described in Appendix A, by Angstmann et al. (2004) and Savukov & Dzuba (2008), with consistent results. We adopt the value of  $q$  from the latter in Table 3 and the quoted error was derived from the spread in the two theoretical values.

## 2.6 Silicon

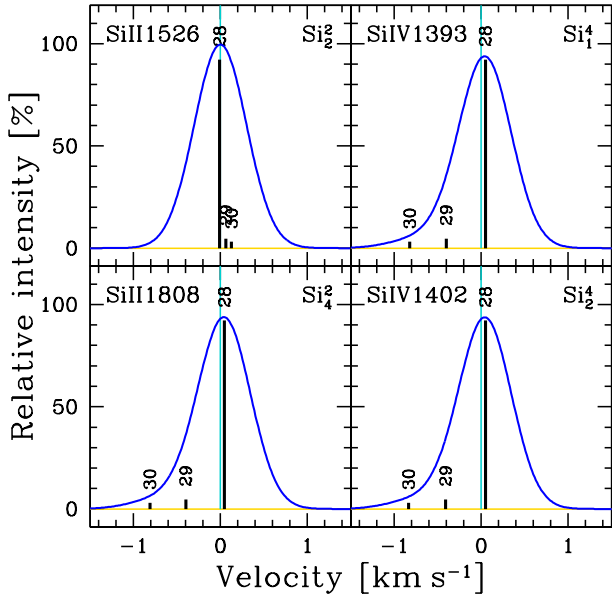
Table 4 summarises the atomic data for the two Si II transitions with precisely-measured laboratory wavelengths and the Si IV doublet which is very prominent in quasar absorption spectra. Figure 4 illustrates the isotopic structures for these transitions.

While many ground-state transitions of Si II are known in the far UV, only 4 of the detectably-strong ones occur redwards of H I Lyman- $\alpha$  and are, therefore, useful for varying- $\alpha$  studies. However, the two bluest Si II transitions,  $\lambda 1260$  and  $\lambda 1304$ , do not have precisely-measured laboratory wavelengths (to our knowledge). The two remaining useful transitions, Si II  $\lambda 1526$  and  $\lambda 1808$ , form a very useful pair for varying- $\alpha$  studies due to their very different oscillator strengths: when Si II  $\lambda 1526$  begins to saturate,  $\lambda 1808$  becomes detectable, thereby ensuring that a useful “anchor” line (small  $q$ -coefficient) is nearly always available in the far UV.

Si II and IV likely arise in different astrophysical environments:

**Table 4.** Laboratory data for transitions of Si of interest for quasar absorption-line varying- $\alpha$  studies described in Section 2.6. See Section 2.1 for full descriptions of each column.

Ion	Tran.	$A$	$\omega_0$ [cm <sup>-1</sup> ]	$X$	$\lambda_0$ [Å]	$\delta\nu$ [m s <sup>-1</sup> ]	Lower state	Upper state	ID	IP <sup>-</sup> , IP <sup>+</sup> [eV]	$f$ or %	$q$ [cm <sup>-1</sup> ]
Si II	1526	28.0855	65500.4538(7) <sup>a</sup>	0	1526.706980(16)	3.2	3s <sup>2</sup> 3p <sup>2</sup> P <sub>1/2</sub> <sup>o</sup>	3s <sup>2</sup> 4s <sup>2</sup> S <sub>1/2</sub>	Si <sub>2</sub> <sup>2</sup>	8.15, 16.35	0.133	47 <sup>b</sup> (4)
		30	65500.42585 <sup>b</sup>	3	1526.7076312						3.087%	
		29	65500.43980 <sup>b</sup>	3	1526.7073061						4.683%	
		28	65500.45545 <sup>b</sup>	3	1526.7069415						92.230%	
	1808	28.0855	55309.3404(4) <sup>a</sup>	0	1808.012883(13)	2.2		3s3p <sup>2</sup> D <sub>3/2</sub>	Si <sub>4</sub> <sup>2</sup>		0.00208	526 <sup>b</sup> (16)
		30	55309.49010 <sup>b</sup>	3	1808.0079895						3.087%	
		29	55309.41403 <sup>b</sup>	3	1808.0104763						4.683%	
		28	55309.33165 <sup>b</sup>	3	1808.0131691						92.230%	
Si IV	1393	28.0855	71748.355(2) <sup>a</sup>	0	1393.760177(39)	8.4	2p <sup>6</sup> 3s <sup>2</sup> S <sub>1/2</sub>	2p <sup>6</sup> 3p <sup>2</sup> P <sub>3/2</sub> <sup>o</sup>	Si <sub>1</sub> <sup>4</sup>	33.49, 45.14	0.513	823 <sup>c</sup> (2)
		30	71748.5517 <sup>d</sup>	3	1393.7563570						3.087%	
		29	71748.4513 <sup>d</sup>	3	1393.7583075						4.683%	
		28	71748.3435 <sup>d</sup>	3	1393.7604003						92.230%	
	1402	28.0855	71287.376(2) <sup>a</sup>	0	1402.772912(39)	8.4		2p <sup>6</sup> 3p <sup>2</sup> P <sub>1/2</sub> <sup>o</sup>	Si <sub>2</sub> <sup>4</sup>		0.254	361 <sup>c</sup> (2)
		30	71287.5743 <sup>d</sup>	3	1402.7690089						3.087%	
		29	71287.4731 <sup>d</sup>	3	1402.7710015						4.683%	
		28	71287.3644 <sup>d</sup>	3	1402.7731393						92.230%	

References: <sup>a</sup>Griesmann & Kling (2000); <sup>b</sup>This work; <sup>c</sup>Dzuba & Johnson (2007); <sup>d</sup>Berengut et al. (2003).**Figure 4.** Si transition isotopic structures in Table 4 described in Section 2.6. See Section 2.1 for Figure details.

given the ionization potentials shown in Table 4, Si II will be the dominant ion in self-shielded, predominantly neutral gas while Si IV will be much more prominent in more diffuse, fairly highly-ionized gas. The highest optical depth velocity components in a Si II absorption profile are therefore unlikely to also have relatively high optical depth in Si IV. They may not even be detectable. Therefore, Si IV absorption lines generally cannot be fit with the same velocity structure as the many singly-ionized species in varying- $\alpha$  studies. Instead, the Si IV doublet is used in the “alkali doublet method” for constraining variations in  $\alpha$  (e.g. Cowie & Songaila 1995; Varshalovich et al. 1996; Murphy et al. 2001c). The ubiquity of the Si IV doublet transitions and the relatively large difference between their  $q$ -coefficients makes this is one of the best doublets for this purpose.

The laboratory wavenumbers for the Si II and IV transitions in

Table 4 were measured by Griesmann & Kling (2000) using the same FTS and Penning discharge lamp setup and scans in which they measured Al II  $\lambda$ 1670. That is, the Si II/IV and Al II  $\lambda$ 1670 wavenumbers are all on the same wavenumber scale which was calibrated with the Whaling et al. (1995) Ar II measurements. The velocity precision achieved is nevertheless better than for Al II  $\lambda$ 1670:  $\sim 3$  m s<sup>-1</sup> for the Si II transitions and  $\sim 8$  m s<sup>-1</sup> even for the highly excited Si IV lines. We are not aware of any subsequent, similarly-precise measurements of these Si II and IV transitions.

There exist no measurements of the isotopic structures for the Si II and IV transitions in Table 4, to our knowledge. Berengut et al. (2003) calculated the specific mass shift ( $k_{\text{SMS}}$ ) for Si II  $\lambda$ 1526 and the Si IV doublet, finding that for the former it opposed the normal mass shift ( $k_{\text{NMS}}$ ), nearly cancelling it out. Therefore, it is important to estimate the field shift ( $F_{\text{FS}}$ ) to better understand the likely isotopic structure of Si II  $\lambda$ 1526. We are not aware of a previous calculation of Si II  $\lambda$ 1808’s isotopic structure. As a rough approximation, previous varying- $\alpha$  studies (e.g. Murphy et al. 2001b, 2003) estimated it by scaling the specific mass shift of the Mg II doublet. By comparison, Si IV’s isotopic structure is simpler to calculate, with the expectation that the results are more reliable. Thus, we have used the results of Berengut et al. (2003) for the Si IV doublet in Table 4. Note the similarity of the Si IV structures in Fig. 4, implying that alkali doublet method varying- $\alpha$  constraints using it are very insensitive to isotopic abundance variations between the laboratory and quasar absorption clouds.

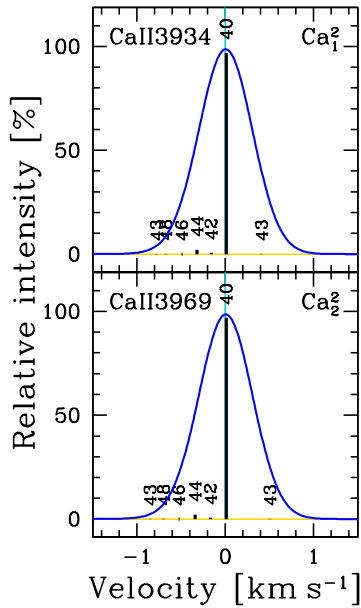
To remedy the situation for Si II we have undertaken new *ab initio* calculations of isotopic structures for a variety of its transitions in Appendix A. The same calculations also yield new  $q$  coefficients, derived with a similar and consistent approach as that used for the  $q$  coefficients of the other species studied here. The detailed results for Si II are presented in Table A1 and the new isotopic structures and  $q$  coefficients are provided in Table 4 and illustrated in Fig. 4. These calculations confirm that the field shift for Si II  $\lambda$ 1526 is a relatively small effect, leaving the expected near-cancellation between the normal and specific mass shifts to provide a very narrow isotopic splitting. The Si II  $\lambda$ 1808 isotopic splitting,  $c\delta\nu^{30,28}/\nu = 0.86$  km s<sup>-1</sup> is also very similar to that assumed by, e.g., Murphy et al. (2003), 0.63 km s<sup>-1</sup>.



**Table 5.** Laboratory data for transitions of Ca of interest for quasar absorption-line varying- $\alpha$  studies described in Section 2.7. See Section 2.1 for full descriptions of each column.

Ion	Tran.	$A$	$\omega_0$ [cm <sup>-1</sup> ]	$X$	$\lambda_0$ [Å]	$\delta v$ [m s <sup>-1</sup> ]	Lower state	Upper state	ID	IP <sup>-</sup> , IP <sup>+</sup> [eV]	$f$ or %	$q$ [cm <sup>-1</sup> ]		
Ca II	3934	40.0780	25414.416438(86)	1	3934.774589(13)	1.0	4s <sup>2</sup> S <sub>1/2</sub>	4p <sup>2</sup> P <sub>3/2</sub> <sup>o</sup>	Ca <sub>1</sub> <sup>2</sup>	6.11, 11.87	0.6267	446 <sup>a</sup> (6)		
		48	25414.4735(42) <sup>b,c,d</sup>	2	3934.76575(65)	49						0.187%		
		46	25414.4583(33) <sup>b,c,d</sup>	2	3934.76811(51)	38						0.004%		
		44	25414.4436(23) <sup>b,c,d</sup>	2	3934.77038(35)	27						2.086%		
		43	25414.38165(73) <sup>e,b,c,f</sup>	2	3934.77998(11)	8.6	$F = 3$	$F = 2, 3, 4$				0.059%		
		43	25414.48235(73) <sup>e,b,c,f</sup>	2	3934.76438(11)	8.6	$F = 4$	$F = 3, 4, 5$				0.076%		
		42	25414.4301(12) <sup>b,c,d</sup>	2	3934.77248(18)	14						0.647%		
		40	25414.415619(17) <sup>d</sup>	0	3934.7747160(26)	0.20						96.941%		
		3969	40.0780	25191.520729(66)	1	3969.589652(10)	0.79			4p <sup>2</sup> P <sub>1/2</sub> <sup>o</sup>	Ca <sub>2</sub> <sup>2</sup>		0.3116	222 <sup>a</sup> (2)
				48	25191.5794(42) <sup>b,c,g</sup>	2	3969.58041(66)	50						0.187%
46	25191.5652(33) <sup>b,c,g</sup>			2	3969.58264(51)	39						0.004%		
44	25191.5496(23) <sup>b,c,g</sup>			2	3969.58510(36)	27						2.086%		
43	25191.47818(46) <sup>e,b,c,f</sup>			2	3969.59636(7)	5.5	$F = 3$	$F = 3, 4$				0.059%		
43	25191.59225(46) <sup>e,b,c,f</sup>			2	3969.57838(7)	5.5	$F = 4$	$F = 3, 4$				0.076%		
42	25191.5348(12) <sup>b,c,g</sup>			2	3969.58743(19)	14						0.647%		
40	25191.519868(57) <sup>g</sup>			0	3969.5897875(89)	0.67						96.941%		

References: <sup>a</sup>Dzuba & Johnson (2007); <sup>b</sup>Maleki & Goble (1992); <sup>c</sup>Mårtensson-Pendrill et al. (1992); <sup>d</sup>Wolf et al. (2009); <sup>e</sup>Arbes et al. (1994); <sup>f</sup>Nörtershäuser et al. (1998); <sup>g</sup>Wolf et al. (2008).

**Figure 5.** Ca transition isotopic and hyperfine structures in Table 5 described in Section 2.7. See Section 2.1 for Figure details.

## 2.7 Calcium

Table 5 shows the atomic data for the two strongest Ca II transitions which are common, though often not particularly strong, in quasar absorption systems (e.g. Zych et al. 2009). Figure 5 illustrates the isotopic and hyperfine structures for these transitions. The Ca II  $\lambda\lambda 3934/3969$  doublet, or K and H transitions are observable at redshifts  $z \lesssim 1.5$  in optical quasar absorption spectra. However, like the Na I  $\lambda\lambda 5891/5897$  doublet, they have not been used so far in varying- $\alpha$  studies (to our knowledge) for the same two main reasons: weak absorption compared to the ubiquitous Mg and Fe II transitions at the same  $z$  and, often, significant telluric contamination. They are nevertheless  $\geq 100$  times stronger than other known Ca II transitions (Morton 2003), so they are the only ones

suitable for varying- $\alpha$  work. Ca has 6 stable isotopes, <sup>40–48</sup>Ca, only one of which has an odd nucleon number (43). All the isotopic splittings, and the significant hyperfine splittings for transitions of the latter, have been measured with adequate precision for high-resolution quasar absorption studies (see below).

Absolute frequencies were recently measured for the <sup>40</sup>Ca II H and K lines by Wolf et al. (2008) and Wolf et al. (2009), respectively, using frequency-comb spectroscopy techniques. The isotopic splittings were measured by Mårtensson-Pendrill et al. (1992) and Maleki & Goble (1992). We averaged the two measurements for each isotope and transition, weighting the average by the inverse-square uncertainties (including the 2 MHz per mass unit difference from <sup>44</sup>Ca systematic error quoted by Mårtensson-Pendrill et al. 1992). The magnetic dipole hyperfine constant ( $A$ ) for the ground state was measured by Arbes et al. (1994), while Nörtershäuser et al. (1998) measured the  $A$  values for the H and K excited states and also the electric quadrupole hyperfine constant ( $B$ ) for the  $\lambda 3934$  excited state. The hyperfine structure was then determined using equations (6)–(10). In Table 5 we simplify the hyperfine structure by averaging over the splitting of the excited states. This is justified for applications in high-resolution spectroscopy because the excited state splitting ( $\sim 200$  m s<sup>-1</sup>) is much smaller than the ground-state splitting ( $\sim 1.5$  km s<sup>-1</sup>) and the isotopic abundance of <sup>43</sup>Ca is very small, just 0.14%. Finally, the composite frequencies were determined from the isotopic and hyperfine component frequencies via equation (3).

Despite the isotopic/hyperfine structures for the Ca II H and K lines illustrated in Fig. 1 being relatively broad ( $\sim 1$  km s<sup>-1</sup>), the final line shape remains almost symmetric and centered very close ( $\sim 10$  km s<sup>-1</sup>) to the <sup>40</sup>Ca isotopic components because they have by far the highest (terrestrial) isotopic abundance (96.9%; Rosman & Taylor 1998). However, if the isotopic abundances of Ca are very different in high-redshift quasar absorption systems, modelling of Ca II profiles with the terrestrial abundances may lead to spurious line-shifts. We are not aware of any theoretical work that provides basic expectations for Ca in this regard, unlike the other species considered in this paper (Fenner et al. 2005).

**Table 6.** Laboratory data for transitions of Ti of interest for quasar absorption-line varying- $\alpha$  studies described in Section 2.8. See Section 2.1 for full descriptions of each column.

Ion	Tran.	A	$\omega_0$ [cm <sup>-1</sup> ]	X	$\lambda_0$ [Å]	$\delta v$ [m s <sup>-1</sup> ]	Lower state	Upper state	ID	IP <sup>-</sup> , IP <sup>+</sup> [eV]	f or %	q [cm <sup>-1</sup> ]
Ti II	1910.6	47.867	52339.240(1) <sup>a</sup>	0	1910.61238(4)	5.7	3d <sup>2</sup> 4s a <sup>4</sup> F <sub>3/2</sub>	3d4s4p <sup>4</sup> D <sup>o</sup> <sub>1/2</sub>	Ti <sub>4</sub> <sup>2</sup>	6.82, 13.58	0.104	-1414 <sup>b</sup> (170)
		50	52339.1552 <sup>b</sup>	3	1910.615477						5.18%	
		49	52339.1943 <sup>b</sup>	3	1910.614051						5.41%	
		48	52339.2361 <sup>b</sup>	3	1910.612524						73.72%	
		47	52339.2785 <sup>b</sup>	3	1910.610976						7.44%	
	46	52339.3233 <sup>b</sup>	3	1910.609339	8.25%							
	1910.9	47.867	52329.889(1) <sup>a</sup>	0	1910.95380(4)	5.7		3d4s4p <sup>4</sup> F <sup>o</sup> <sub>3/2</sub>	Ti <sub>5</sub> <sup>2</sup>		0.0980	-1689 <sup>b</sup> (250)
		50	52329.8057 <sup>b</sup>	3	1910.956836						5.18%	
		49	52329.8441 <sup>b</sup>	3	1910.955436						5.41%	
		48	52329.8852 <sup>b</sup>	3	1910.953935						73.72%	
		47	52329.9268 <sup>b</sup>	3	1910.952416						7.44%	
	46	52329.9708 <sup>b</sup>	3	1910.950808	8.25%							
	3067	47.867	32602.6283(14) <sup>c,a,d</sup>	0	3067.23737(13)	13.0		3d <sup>2</sup> 4p z <sup>4</sup> D <sup>o</sup> <sub>3/2</sub>	Ti <sub>7</sub> <sup>2</sup>		0.0489	855 <sup>b</sup> (80)
		50	32602.65258 <sup>b</sup>	3	3067.235089						5.18%	
		49	32602.64187 <sup>b</sup>	3	3067.236097						5.41%	
		48	32602.62930 <sup>b</sup>	3	3067.237279						73.72%	
		47	32602.61768 <sup>b</sup>	3	3067.238373						7.44%	
	46	32602.60483 <sup>b</sup>	3	3067.239582	8.25%							
	3073	47.867	32532.3566(7) <sup>c,a,d</sup>	0	3073.86278(7)	6.5		3d <sup>2</sup> 4p z <sup>4</sup> D <sup>o</sup> <sub>1/2</sub>	Ti <sub>3</sub> <sup>2</sup>		0.121	739 <sup>b</sup> (80)
		50	32532.38075 <sup>b</sup>	3	3073.860495						5.18%	
49		32532.37011 <sup>b</sup>	3	3073.861501	5.41%							
48		32532.35759 <sup>b</sup>	3	3073.862683	73.72%							
47		32532.34604 <sup>b</sup>	3	3073.863774	7.44%							
46	32532.33325 <sup>b</sup>	3	3073.864983	8.25%								
3230	47.867	30958.5871(10) <sup>c,d</sup>	0	3230.12157(10)	9.7		3d <sup>2</sup> 4p z <sup>4</sup> F <sup>o</sup> <sub>5/2</sub>	Ti <sub>6</sub> <sup>2</sup>		0.0687	721 <sup>b</sup> (70)	
	50	30958.61173 <sup>b</sup>	3	3230.119002						5.18%		
	49	30958.60088 <sup>b</sup>	3	3230.120133						5.41%		
	48	30958.58816 <sup>b</sup>	3	3230.121461						73.72%		
	47	30958.57639 <sup>b</sup>	3	3230.122688						7.44%		
46	30958.56338 <sup>b</sup>	3	3230.124046	8.25%								
3242	47.867	30836.4271(10) <sup>c,d</sup>	0	3242.91785(11)	9.7		3d <sup>2</sup> 4p z <sup>4</sup> F <sup>o</sup> <sub>3/2</sub>	Ti <sub>2</sub> <sup>2</sup>		0.232	563 <sup>b</sup> (30)	
	50	30836.45206 <sup>b</sup>	3	3242.915229						5.18%		
	49	30836.44106 <sup>b</sup>	3	3242.916386						5.41%		
	48	30836.42817 <sup>b</sup>	3	3242.917742						73.72%		
	47	30836.41623 <sup>b</sup>	3	3242.918997						7.44%		
46	30836.40304 <sup>b</sup>	3	3242.920385	8.25%								
3384	47.867	29544.4551(10) <sup>c,d</sup>	0	3384.72988(11)	10.1		3d <sup>2</sup> 4p z <sup>4</sup> G <sup>o</sup> <sub>5/2</sub>	Ti <sub>1</sub> <sup>2</sup>		0.358	408 <sup>b</sup> (30)	
	50	29544.48132 <sup>b</sup>	3	3384.726877						5.18%		
	49	29544.46970 <sup>b</sup>	3	3384.728208						5.41%		
	48	29544.45618 <sup>b</sup>	3	3384.729757						73.72%		
	47	29544.44358 <sup>b</sup>	3	3384.731201						7.44%		
46	29544.42969 <sup>b</sup>	3	3384.732792	8.25%								

References: <sup>a</sup>Ruffoni & Pickering (2010); <sup>b</sup>This work; <sup>c</sup>Aldenius (2009); <sup>d</sup>Nave (2012).

## 2.8 Titanium

Table 6 summarises the atomic data for the seven Ti II transitions with precisely-measured laboratory wavelengths and Fig. 6 illustrates their isotopic structures. To our knowledge, Ti II has not yet been utilized in varying- $\alpha$  studies, mainly because of two factors: the frequencies of the transitions in Table 6 have only recently been measured precisely enough (Aldenius et al. 2006; Ruffoni & Pickering 2010) and Ti has a low abundance in general, some 2.5 orders of magnitude below that of Fe (e.g. Asplund et al. 2009), so it is only detected in quasar absorbers with the strongest metal absorption, and those are the rarest. Nevertheless, the Ti II transitions in Table 6 are a particularly interesting combination for varying- $\alpha$  studies because they have similar oscillator strengths and, most importantly, the pair near 1910 Å have large, negative  $q$ -coefficients whereas the 5 transitions redwards of 3000 Å have moderate, pos-

itive  $q$ -coefficients. That is, within the same ion, transitions are available (with precisely measured laboratory frequencies) which shift in opposite directions to each other as  $\alpha$  varies. This property is shared only by Fe II – see section 2.11. However, aside from identifying absorption systems with strong enough metal absorption to allow high-quality spectra of the Ti II transitions to be obtained, another challenge is that the negative- and positive- $q$  transitions lie so far apart. This could mean that any long-range wavelength mis-calibrations of the quasar spectra may play an important role and it limits the number of quasar absorbers where all the Ti II transitions in Table 6 can be detected outside the Lyman- $\alpha$  forest.

The wavenumbers for the 5 Ti II transitions redwards of 3000 Å were measured with  $\sim 10$  m s<sup>-1</sup> precision by Aldenius et al. (2006) (see also Aldenius 2009) using a FTS and HCL. The wavenumbers were calibrated using the Ar II scale of Whaling et al. (1995). However, following the comprehensive re-calibration

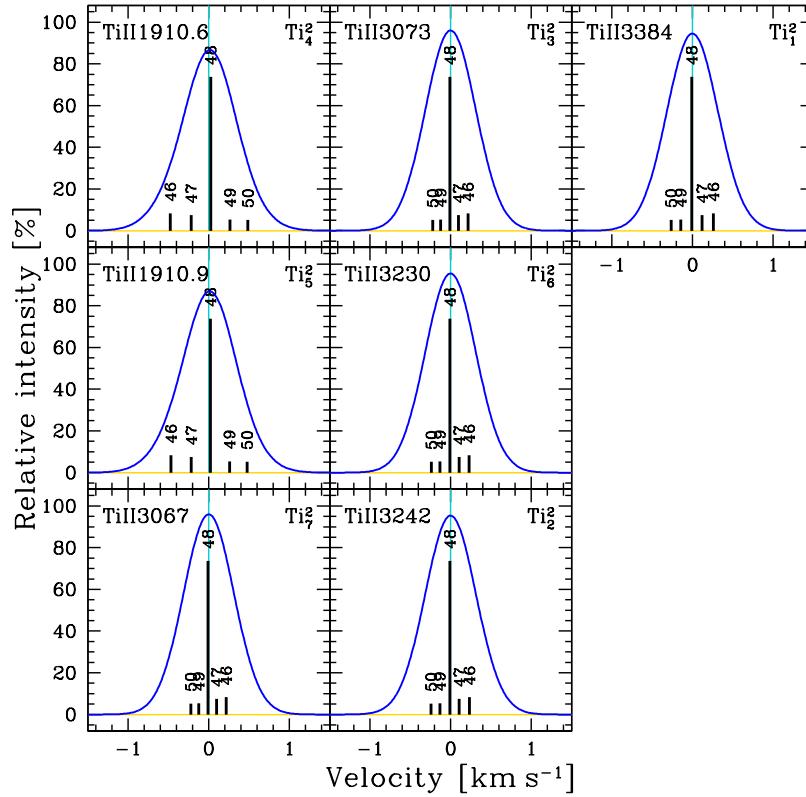


Figure 6. Ti transition isotopic structures in Table 6 described in Section 2.8. See Section 2.1 for Figure details.

analysis of Nave & Sansonetti (2011), the wavenumbers of Aldenius (2009) were increased by 3.7 parts per  $10^8$  by Nave (2012). For the Ti II  $\lambda$ 3230,  $\lambda$ 3243 and  $\lambda$ 3384 transitions, these increased wavenumbers are the composite values reported in Table 6.

The wavenumbers for the pair of Ti II transitions at 1910 Å and the  $\lambda$ 3067/3073 doublet were measured by Ruffoni & Pickering (2010) with  $\sim 10$ – $20$  m s $^{-1}$  precision using a FTS and HCL. Again, the wavenumbers were calibrated using the Ar II scale of Whaling et al. (1995). However, the Mg I  $\lambda$ 2026 and  $\lambda$ 2852 transitions discussed in section 2.4 were recorded simultaneously as calibration standards. Ruffoni & Pickering found that their Ar II-calibrated Mg I wavenumbers agreed well with the frequency-comb based, absolute measurements of Hannemann et al. (2006) and Salumbides et al. (2006). Ruffoni & Pickering’s Ti II  $\lambda$ 3067/3073 doublet wavenumbers also agree with the corrected Aldenius (2009) values reported by Nave (2012). Therefore, we adopt a simple weighted mean wavenumber for the composite values reported in Table 6 for the  $\lambda$ 3067/3073 doublet. For the  $\lambda$ 1910.6 and  $\lambda$ 1910.9 transitions, we adopt Ruffoni & Pickering’s wavenumbers.

To our knowledge, there exists no measurements of the isotopic structures for the Ti II transitions in Table 6. Berengut et al. (2008) calculated the total isotopic shifts for the 5 transitions redwards of 3000 Å but no previous estimates are available for the pair of transitions at 1910 Å. We have therefore undertaken new *ab initio* isotopic structure and  $q$  coefficient calculations for all 7 Ti II transitions of interest in Appendix A. The detailed results are presented in Table A2 and the new isotopic structures and  $q$  coefficients are provided in Table 6 and illustrated in Fig. 6. The new calculations were very similar to those of Berengut et al. (2008) and we find very similar results for the 5 transitions redwards of 3000 Å. For the pair of transitions at 1910 Å, we find that the iso-

topic structures are reversed, with the heavier isotopes appearing at lower frequencies. This reversal correlates with the reversed sign of the  $q$  coefficients for these transitions. This is very important for varying- $\alpha$  studies: even if the isotopic structures in Fig. 6 are fit to the quasar absorption profiles, any significant deviations from the terrestrial Ti isotopic abundances in the quasar absorbers will lead to spurious line-shift measurements which will mimic a variation in  $\alpha$ .

## 2.9 Chromium

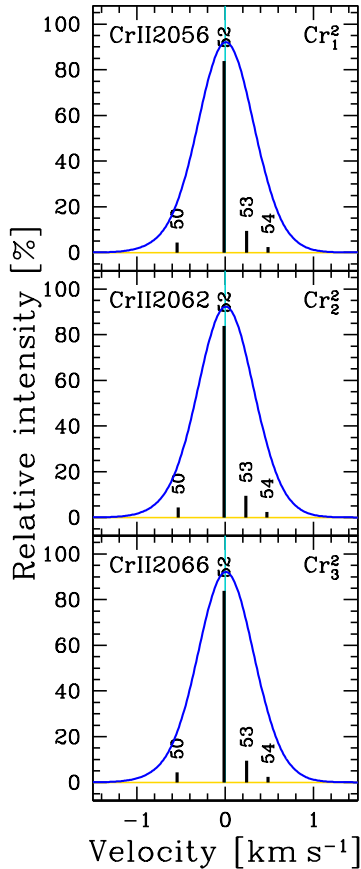
Table 7 summarises the atomic data for the Cr II triplet near 2060 Å and Fig. 7 illustrates their isotopic structures. While several other ground-state transitions of Cr II lie in the UV, redwards of H I Lyman- $\alpha$ ,<sup>2</sup> they are all  $>30$  times weaker than the Cr II triplet near 2060 Å. These three Cr II lines are therefore the most commonly observed in quasar absorption spectra. Nevertheless, they are usually very weak because of the comparatively low abundance of Cr. Thus, even though the Cr II triplet has been used in some varying- $\alpha$  studies, it has generally not provided the dominant constraints (e.g. Murphy et al. 2001b; King et al. 2012). This is despite the remarkable feature that they have fairly large but, most-importantly, negative  $q$ -coefficients.

The Cr II triplet wavenumbers have been measured in two independent analyses with FTSs and HCLs. The wavenumbers measured by Pickering et al. (2000) were calibrated using the older Ar II scale of Norlén (1973), while those measured by Aldenius et al.

<sup>2</sup> Notably Cr II  $\lambda$ 2026 which falls very close to the Mg I and Zn II  $\lambda$ 2026 transitions discussed in sections 2.4 and 2.13, respectively.

**Table 7.** Laboratory data for transitions of Cr of interest for quasar absorption-line varying- $\alpha$  studies described in Section 2.9. See Section 2.1 for full descriptions of each column.

Ion	Tran.	A	$\omega_0$ [ $\text{cm}^{-1}$ ]	X	$\lambda_0$ [ $\text{\AA}$ ]	$\delta v$ [ $\text{m s}^{-1}$ ]	Lower state	Upper state	ID	IP <sup>-</sup> , IP <sup>+</sup> [eV]	f or %	q [ $\text{cm}^{-1}$ ]
Cr II	2056	51.9961	48632.0597(14) <sup>a,b,c</sup>	0	2056.256728(60)	8.7	$3d^5\ ^6S_{5/2}$	$3d^4 4p\ ^6P_{7/2}^o$	Cr <sub>1</sub> <sup>2</sup>	6.77, 16.50	0.103	-1061 <sup>d</sup> (70)
		54	48631.98144 <sup>d</sup>	3	2056.2600379						2.365%	
		53	48632.02086 <sup>d</sup>	3	2056.2583712						9.501%	
		52	48632.06174 <sup>d</sup>	3	2056.2566427						83.789%	
		50	48632.14853 <sup>d</sup>	3	2056.2529732						4.345%	
	2062	51.9961	48491.0583(14) <sup>a,b,c</sup>	0	2062.235873(60)	8.7		$3d^4 4p\ ^6P_{3/2}^o$	Cr <sub>2</sub> <sup>2</sup>		0.0759	-1280 <sup>d</sup> (70)
		54	48490.98199 <sup>d</sup>	3	2062.2391193						2.365%	
		53	48491.02049 <sup>d</sup>	3	2062.2374821						9.501%	
		52	48491.06028 <sup>d</sup>	3	2062.2357899						83.789%	
		50	48491.14471 <sup>d</sup>	3	2062.2321991						4.345%	
	2066	51.9961	48398.8729(14) <sup>a,b,c</sup>	0	2066.163819(60)	8.8		$3d^4 4p\ ^6P_{3/2}^o$	Cr <sub>3</sub> <sup>2</sup>		0.0512	-1421 <sup>d</sup> (70)
		54	48398.79495 <sup>d</sup>	3	2066.1671454						2.365%	
		53	48398.83418 <sup>d</sup>	3	2066.1654706						9.501%	
		52	48398.87486 <sup>d</sup>	3	2066.1637338						83.789%	
		50	48398.96123 <sup>d</sup>	3	2066.1600466						4.345%	

References: <sup>a</sup>Aldenius (2009); <sup>b</sup>Pickering et al. (2000); <sup>c</sup>Nave (2012); <sup>d</sup>Berengut (2011).**Figure 7.** Cr transition isotopic structures in Table 7 described in Section 2.9. See Section 2.1 for Figure details.

(2006) (see also Aldenius 2009) were calibrated using the Whaling et al. (1995) scale. Nave (2012) placed both sets of measurements on a common calibration scale consistent with that of absolute standards derived from frequency comb measurements and we adopt Nave's corrections here. The final composite wavenumbers shown in Table 7 are a simple weighted mean of the corrected values from Pickering et al. (2000) and Aldenius (2009).

There are no measurements of the isotopic structure of the Cr II triplet transitions, to our knowledge. Berengut (2011) calculated the isotopic component separations (their table 6) and we have used these and equation (4) to report the isotopic structures in Table 7. The resulting isotopic splittings are reasonably wide for a relatively heavy ion like Cr II, up to  $\sim 0.55\text{ km s}^{-1}$ . Therefore, if the isotopic abundances in quasar absorbers do not reflect those in the terrestrial environment, spurious line-shifts could be measured for the Cr II transitions. Fenner et al. (2005) explored the isotopic abundances expected in lower-than-solar metallicity environments using a chemical evolution model of a Milky Way-like disc galaxy, finding that the sub-dominant Cr isotopes should be even less abundant at the metallicities typical of the highest column density quasar absorbers. With the composite frequencies and those of the dominant isotope ( $^{52}\text{Cr}$ ) being so similar in the Cr II triplet, this would imply little systematic effect on measurements of  $\alpha$  in quasar absorbers. However, while this might represent the basic theoretical expectation, it is important to recognise that no current constraints on the actual Cr isotopic abundances in quasar absorbers exist.

Our recommended  $q$  coefficients for Cr II in Table 7 are taken from the CI+MBPT calculations of Berengut (2011). These calculations are in good agreement with previous CI calculations (Dzuba et al. 2002).

## 2.10 Manganese

Table 8 summarises the atomic data for Mn II triplet near 2595  $\text{\AA}$  and Fig. 8 illustrates their hyperfine structures. Only 8 transitions of Mn II lie redwards of H I Lyman- $\alpha$  (Morton 2003) and the Mn II triplet are by-far the strongest; they are more than two orders of magnitude stronger than the next strongest transition. Despite having a similar terrestrial abundance to Cr, their higher absolute oscillator strengths (of order 0.2–0.3) make these three Mn II lines more frequently observed in quasar absorption spectra, and more often usable in varying- $\alpha$  analyses. Nevertheless, their laboratory wavenumbers were only measured precisely enough for the first time in 2005, and, to our knowledge, only one study has utilized them to constrain possible variations in  $\alpha$  (King et al. 2012). Like Al, Mn has only one stable isotope ( $^{55}\text{Mn}$ ), making it immune to systematic effects related to isotopic abundance evolution.

The Mn II triplet wavenumbers have been measured in two

**Table 8.** Laboratory data for transitions of Mn of interest for quasar absorption-line varying- $\alpha$  studies described in Section 2.10. See Section 2.1 for full descriptions of each column.

Ion	Tran.	A	$\omega_0$ [cm <sup>-1</sup> ]	X	$\lambda_0$ [Å]	$\delta v$ [m s <sup>-1</sup> ]	Lower state	Upper state	ID	IP <sup>-</sup> , IP <sup>+</sup> [eV]	f or %	q [cm <sup>-1</sup> ]	
Mn II	2576	54.9380	38806.6923(17) <sup>a,b,c</sup>	0	2576.87512(11)	12.9	3d <sup>5</sup> 4s a <sup>7</sup> S <sub>3</sub>	3d <sup>5</sup> 4p z <sup>7</sup> P <sub>4</sub> <sup>o</sup>	Mn <sub>1</sub> <sup>2</sup>	7.44, 15.64	0.361	1276 <sup>d</sup> (150)	
		55	38806.45473	3	2576.890898		$F = 0.5, 1.5$	$F = 1.5, 2.5$			28.571%		
		55	38806.62838	3	2576.879368		$F = 2.5$	$F = 1.5, 2.5, 3.5$			23.801%		
		55	38806.77173	3	2576.869849		$F = 3.5$	$F = 2.5, 3.5, 4.5$			19.030%		
		55	38806.88249	3	2576.862494		$F = 4.5$	$F = 3.5, 4.5, 5.5$			14.286%		
	55	38806.97756	3	2576.856181		$F = 5.5$	$F = 4.5, 5.5, 6.5$			14.312%			
	2594	54.9380	38543.1250(17) <sup>a,b,c</sup>	0	2594.49643(11)	12.9		3d <sup>5</sup> 4p z <sup>7</sup> P <sub>3</sub> <sup>o</sup>	Mn <sub>2</sub> <sup>2</sup>			0.280	1030 <sup>d</sup> (150)
		55	38542.89261	3	2594.512068		$F = 0.5, 1.5$	$F = 0.5, 1.5, 2.5$			28.579%		
		55	38543.06316	3	2594.500587		$F = 2.5$	$F = 1.5, 2.5, 3.5$			23.841%		
		55	38543.20275	3	2594.491191		$F = 3.5$	$F = 2.5, 3.5, 4.5$			19.078%		
		55	38543.31105	3	2594.483901		$F = 4.5$	$F = 3.5, 4.5, 5.5$			14.289%		
	55	38543.40454	3	2594.477608		$F = 5.5$	$F = 4.5, 5.5$			14.213%			
	2606	54.9380	38366.2313(17) <sup>a,b,c</sup>	0	2606.45877(11)	13.0		3d <sup>5</sup> 4p z <sup>7</sup> P <sub>2</sub> <sup>o</sup>	Mn <sub>3</sub> <sup>2</sup>			0.198	869 <sup>d</sup> (150)
		55	38365.94424	3	2606.478271		$F = 0.5, 1.5$	$F = 0.5, 1.5, 2.5$			28.563%		
		55	38366.15463	3	2606.463977		$F = 2.5$	$F = 1.5, 2.5, 3.5$			23.793%		
55		38366.32705	3	2606.452264		$F = 3.5$	$F = 2.5, 3.5, 4.5$			19.052%			
55		38366.46082	3	2606.443176		$F = 4.5$	$F = 3.5, 4.5$			14.282%			
55	38366.57520	3	2606.435406		$F = 5.5$	$F = 4.5$			14.310%				

References: <sup>a</sup>Aldenius (2009); <sup>b</sup>Blackwell-Whitehead et al. (2005); <sup>c</sup>Nave (2012); <sup>d</sup>Berengut et al. (2004).

independent analyses using FTSs with HCLs. The wavenumbers measured by Blackwell-Whitehead et al. (2005) were calibrated using the older Ar II scale of Norlén (1973), while those measured by Aldenius et al. (2006) (see also Aldenius 2009) were calibrated using the Whaling et al. (1995) scale. Following the analysis of Nave & Sansonetti (2011), Nave (2012) concluded that Aldenius' wavenumbers should be increased by 3.7 parts in 10<sup>8</sup>, but no reference is made to Blackwell-Whitehead et al.'s wavenumbers. However, the calibration procedure of Blackwell-Whitehead et al. and Pickering et al. (2000) appear to be the same, and Nave (2012) conclude that Pickering et al.'s wavenumbers should be increased by 10.6 parts in 10<sup>8</sup>, so we adopt the same correction here for Blackwell-Whitehead et al.'s wavenumbers. With both sets of Mn II corrected to the same wavenumber scale as above – that equivalent to the Ar II Whaling et al. (1995) scale consistent with the absolute scale derived from frequency comb measurements – we adopt the weighted mean composite wavenumbers in Table 8.

The FTS spectra of both Blackwell-Whitehead et al. (2005) and Aldenius (2009) resolve significant hyperfine structure in the Mn II triplet transitions. <sup>55</sup>Mn has a relatively large magnetic dipole moment ( $\mu = +3.5$  nuclear magnetons), so many observable Mn transitions in stellar spectra have prominent hyperfine structure. Indeed, ignoring the hyperfine structure of Mn transitions can lead to substantial systematic errors in stellar elemental abundances (e.g. Prochaska & McWilliam 2000), sometimes as much as one or two orders of magnitude (Jomaron et al. 1999).

Blackwell-Whitehead et al. (2005) first calculated the hyperfine structure for the Mn II ground state. With a nuclear spin of  $I = 5/2$ , the ground state contains 6 hyperfine levels with half-integer total angular momenta,  $F = \frac{1}{2} - \frac{11}{2}$ . Given the triplet excited state electronic configurations and selection rules, the three Mn II transitions have a total of 14–16 hyperfine components each. Blackwell-Whitehead et al. determined the hyperfine structure constants ( $A$  and  $B$ ) by fitting their FTS spectra with their calculated structure, finding that ground state splitting dominated the excited state splitting. Therefore, in Table 8 we group together the hyperfine components from each ground state and provide their com-

posite wavenumber. We also grouped together the two lowest-lying ground states ( $F = \frac{1}{2}$  &  $\frac{3}{2}$ ) because their wavenumbers differed relatively little; that is, each Mn II is represented by 5 grouped hyperfine components in Table 8. We scaled these grouped component wavenumbers to ensure that their composite value [equation (4)] agreed with the weighted mean composite wavenumber from the two different FTS studies for each transition in Table 8.

The recommended  $q$  coefficients for Mn II in Table 8 are taken from the AMBiT CI calculations of Berengut et al. (2004). The older CI calculations of Dzuba et al. (1999a) are consistent within the stated uncertainties.

## 2.11 Iron

Table 9 presents the available atomic data for 10 Fe II lines falling redwards of H I Lyman- $\alpha$ . The isotopic structures calculated by Porsev et al. (2009) for nine of these transitions are illustrated in Fig. 9. One weak transition ( $f = 0.024$ ) with a precisely measured laboratory wavelength, 1260.53557(6) Å (Nave 2012), currently lacks a calculated  $q$  coefficient, so is not shown in Table 9. In practice, that transition is often comprehensively blended with the very strong Si II transition at 1260.4221 Å, rendering it unusable for varying  $\alpha$  analyses except when the velocity structure of the absorber spans  $<27$  km s<sup>-1</sup>. A further 4 very weak Fe II transitions lie redwards of H I Lyman- $\alpha$  which are stronger than the weakest transition we list in Table 9 – i.e. with oscillator strengths  $2.5 \times 10^{-5} < f < 1.5 \times 10^{-4}$  – and which have precisely-measured (vacuum) wavelengths: 2234.44624(9), 1901.76075(9), 1620.06106(7) and 1588.68741(6) Å (Nave & Johansson 2013). These transitions also currently lack calculated  $q$  coefficients, so we consider them no further here.

Transitions of Fe I are very rarely observed in quasar absorbers because, with its low ionization potential (7.87 eV), it has a very low abundance compared with Fe II. However,  $q$  coefficients for many Fe I transitions have been calculated because some were observed towards some bright quasars (Dzuba & Flambaum 2008; Porsev et al. 2009). Indeed, of the 13 strongest Fe I transitions listed

**Table 9.** Laboratory data for transitions of Fe of interest for quasar absorption-line varying- $\alpha$  studies described in Section 2.11. See Section 2.1 for full descriptions of each column.

Ion	Tran.	A	$\omega_0$ [cm <sup>-1</sup> ]	X	$\lambda_0$ [Å]	$\delta\nu$ [m s <sup>-1</sup> ]	Lower state	Upper state	ID	IP <sup>-</sup> , IP <sup>+</sup> [eV]	f or %	q [cm <sup>-1</sup> ]
Fe II	1608	55.845	62171.623(3) <sup>a</sup>	0	1608.450852(78)	14.5	3d <sup>6</sup> 4s a <sup>6</sup> D <sub>9/2</sub>	3d <sup>5</sup> 4s4p y <sup>6</sup> P <sub>7/2</sub> <sup>o</sup>	Fe <sub>5</sub> <sup>2</sup>	7.87, 16.18	0.0577	-1165 <sup>b,c</sup> (300)
		58	62171.57878 <sup>c</sup>	3	1608.4519963						0.282%	
		57	62171.59948 <sup>c</sup>	3	1608.4514606						2.119%	
		56	62171.62093 <sup>c</sup>	3	1608.4509059						91.754%	
		54	62171.66620 <sup>c</sup>	3	1608.4497347						5.845%	
	1611	55.845	62065.527(3) <sup>a</sup>	0	1611.200369(78)	14.5		3d <sup>6</sup> 4p y <sup>4</sup> F <sub>7/2</sub> <sup>o</sup>	Fe <sub>10</sub> <sup>2</sup>		0.00138	1330 <sup>b,c</sup> (300)
		58	62065.55558 <sup>c</sup>	3	1611.1996271						0.282%	
		57	62065.54220 <sup>c</sup>	3	1611.1999744						2.119%	
		56	62065.52834 <sup>c</sup>	3	1611.2003342						91.754%	
		54	62065.49909 <sup>c</sup>	3	1611.2010936						5.845%	
	2249	55.845	44446.9044(19) <sup>a</sup>	0	2249.875472(96)	12.8		3d <sup>6</sup> 4p z <sup>4</sup> D <sub>7/2</sub> <sup>o</sup>	Fe <sub>9</sub> <sup>2</sup>		0.00182	1604 <sup>d</sup> (200)
		58	44446.93584 <sup>c</sup>	3	2249.8738801						0.282%	
		57	44446.92112 <sup>c</sup>	3	2249.8746253						2.119%	
		56	44446.90587 <sup>c</sup>	3	2249.8753970						91.754%	
		54	44446.87369 <sup>c</sup>	3	2249.8770263						5.845%	
	2260	55.845	44232.5390(19) <sup>e,a</sup>	0	2260.779108(97)	12.9		3d <sup>6</sup> 4p z <sup>4</sup> F <sub>9/2</sub> <sup>o</sup>	Fe <sub>8</sub> <sup>2</sup>		0.00244	1435 <sup>d</sup> (150)
	2344	55.845	42658.2443(14) <sup>e,a</sup>	0	2344.212747(76)	9.7		3d <sup>6</sup> 4p z <sup>6</sup> P <sub>7/2</sub> <sup>o</sup>	Fe <sub>3</sub> <sup>2</sup>		0.114	1375 <sup>b,c</sup> (300)
		58	42658.26949 <sup>c</sup>	3	2344.2113616						0.282%	
		57	42658.25768 <sup>c</sup>	3	2344.2120103						2.119%	
		56	42658.24546 <sup>c</sup>	3	2344.2126822						91.754%	
		54	42658.21964 <sup>c</sup>	3	2344.2141007						5.845%	
	2367	55.845	42237.0563(19) <sup>a</sup>	0	2367.58924(11)	13.5		3d <sup>6</sup> 4p z <sup>6</sup> F <sub>7/2</sub> <sup>o</sup>	Fe <sub>15</sub> <sup>2</sup>		0.0000216	1803 <sup>d</sup> (200)
		58	42237.08770 <sup>c</sup>	3	2367.587479						0.282%	
		57	42237.07300 <sup>c</sup>	3	2367.588303						2.119%	
		56	42237.05777 <sup>c</sup>	3	2367.589157						91.754%	
		54	42237.02563 <sup>c</sup>	3	2367.590959						5.845%	
	2374	55.845	42114.8376(14) <sup>e,a</sup>	0	2374.460064(78)	9.8		3d <sup>6</sup> 4p z <sup>6</sup> F <sub>9/2</sub> <sup>o</sup>	Fe <sub>6</sub> <sup>2</sup>		0.03130	1625 <sup>b,c</sup> (100)
		58	42114.86890 <sup>c</sup>	3	2374.4582998						0.282%	
57		42114.85425 <sup>c</sup>	3	2374.4591258	2.119%							
56		42114.83907 <sup>c</sup>	3	2374.4599813	91.754%							
54		42114.80704 <sup>c</sup>	3	2374.4617873	5.845%							
2382	55.845	41968.0674(14) <sup>e,a</sup>	0	2382.763995(80)	10.1		3d <sup>6</sup> 4p z <sup>6</sup> F <sub>11/2</sub> <sup>o</sup>	Fe <sub>1</sub> <sup>2</sup>		0.320	1505 <sup>b,c</sup> (100)	
	58	41968.09852 <sup>c</sup>	3	2382.7622294						0.282%		
	57	41968.08396 <sup>c</sup>	3	2382.7630560						2.119%		
	56	41968.06888 <sup>c</sup>	3	2382.7639122						91.754%		
	54	41968.03705 <sup>c</sup>	3	2382.7657196						5.845%		
2586	55.845	38660.0532(13) <sup>e,a</sup>	0	2586.649312(87)	10.0		3d <sup>6</sup> 4p z <sup>6</sup> D <sub>7/2</sub> <sup>o</sup>	Fe <sub>4</sub> <sup>2</sup>		0.0691	1515 <sup>b,c</sup> (100)	
	58	38660.07931 <sup>c</sup>	3	2586.6475648						0.282%		
	57	38660.06708 <sup>c</sup>	3	2586.6483830						2.119%		
	56	38660.05441 <sup>c</sup>	3	2586.6492304						91.754%		
	54	38660.02768 <sup>c</sup>	3	2586.6510194						5.845%		
2600	55.845	38458.9926(13) <sup>e,a</sup>	0	2600.172114(88)	10.1		3d <sup>6</sup> 4p z <sup>6</sup> D <sub>9/2</sub> <sup>o</sup>	Fe <sub>2</sub> <sup>2</sup>		0.239	1370 <sup>b,c</sup> (100)	
	58	38459.01850 <sup>c</sup>	3	2600.1703603						0.282%		
	57	38459.00636 <sup>c</sup>	3	2600.1711816						2.119%		
	56	38458.99377 <sup>c</sup>	3	2600.1720322						91.754%		
	54	38458.96721 <sup>c</sup>	3	2600.1738281						5.845%		

References: <sup>a</sup>Nave (2012); <sup>b</sup>Dzuba et al. (2002); <sup>c</sup>Porsev et al. (2009); <sup>d</sup>Berengut (2006); <sup>e</sup>Aldenius (2009).

by Morton (2003), spanning a factor of 25 in oscillator strength, 11 have known  $q$  coefficients (with up to ~40% uncertainties)<sup>3</sup>. However, we do not consider them here because, unfortunately, their

laboratory frequencies are not known with high enough precision to meet our  $\delta\nu \lesssim 20 \text{ km s}^{-1}$  criterion.

Wavenumbers for the six strongest Fe II lines in Table 9, all at laboratory wavelengths >2260 Å, were measured by Aldenius et al. (2006) (see also Aldenius 2009) using an FTS and HCL. Wavenumbers for all the transitions in Table 9 were also previously measured with different FTSs (and HCLs), as described in Nave (2012). Nave & Sansonetti (2011) considered in detail the wavelength calibration scales of all these measurements and recommended corrections to their measured wavenumbers to place them on the Ar II Whaling et al. (1995) scale which is consistent with the absolute scale de-

<sup>3</sup> These 13 Fe I transitions' frequencies were presented by Nave et al. (1994) and corrected (upwards by 6.7 parts in 10<sup>8</sup>) by Nave & Sansonetti (2011) to give the following vacuum wavelengths (in decreasing oscillator strength order): 2484.0207(6), 2523.6081(3), 2167.4532(5), 2719.8328(4), 3021.5185(5), 2463.3920(3), 2501.8857(3), 2967.7644(4), 3720.9926(7), 2984.4400(4), 2298.8767(3), 3441.5917(6), 3861.0055(7) Å.

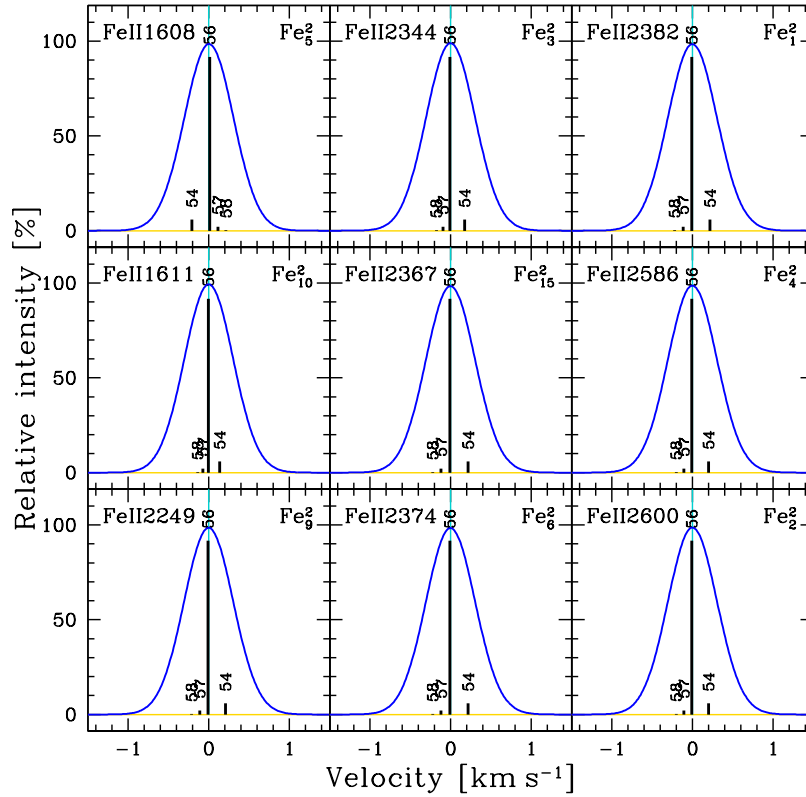


**Figure 9.** Fe transition isotopic structures in Table 9 described in Section 2.11. See Section 2.1 for Figure details.

rived from frequency comb measurements. In particular, they conclude that Aldenius’ wavenumbers should be increased by 3.7 parts in  $10^8$ . Nave (2012) also used a comprehensive energy level analysis to derive more precise Ritz wavenumbers for the Fe II transitions in Table 9. We adopt those Ritz composite wavenumbers here. For the six strongest transitions, we adopt the weighted mean of Nave’s value and the increased Aldenius (2009) value as the composite wavenumber in Table 9.

To our knowledge, no measurements exist of the isotopic structure of the Fe II transitions in Table 9. Porsev et al. (2009) calculated the specific mass shift constant ( $k_{\text{SMS}}$ ) for all but the  $\lambda 2260$  transition. General agreement was found with the earlier calculations of Kozlov et al. (2004), though the systematic uncertainties were still estimated to  $\geq 20\%$ . Assuming the field shift term in equation (5) to be small, we neglect it and use Porsev et al.’s  $k_{\text{SMS}}$  values to report the isotopic structures in Table 9. The results are illustrated in Fig. 9. Given the considerable uncertainties, and that the field shifts are ignored here, these structures should only be treated as representative of what can be expected. Of particular note is that the calculated isotopic structures are very compact, spanning only  $\sim 400 \text{ m s}^{-1}$ , compared with those of other transitions discussed in this paper. This implies that Fe II isotopic structure effects should not be important for varying  $\alpha$  analyses. However, note that the isotopic structure of the  $\lambda 1608$  transition is reversed relative to the others in Fig. 9; heavier isotopes have *longer*  $\lambda 1608$  transition wavelengths. This means that if the relative Fe isotopic abundances in a quasar absorption system differ from the terrestrial values used to model the absorption profiles, the effect on the line centroids will be almost completely degenerate with a shift in  $\alpha$ . For example, from Fig. 9 it is immediately clear that if the  $^{54}\text{Fe}/^{56}\text{Fe}$  ratio was inverted in quasar absorbers compared to the

terrestrial value (i.e. 15.7 instead of 0.064), but the terrestrial ratio was assumed in fits to the Fe II transitions, a spurious velocity shift of  $\sim 400 \text{ m s}^{-1}$  would be measured between the Fe II  $\lambda 1608$  transition and the other Fe II transitions in Table 9. While much less extreme Fe isotopic abundance differences are expected in quasar absorbers (Fenner et al. 2005), this example illustrates how using only Fe II transitions in varying  $\alpha$  analyses is not immune to systematic errors from isotopic abundance evolution.

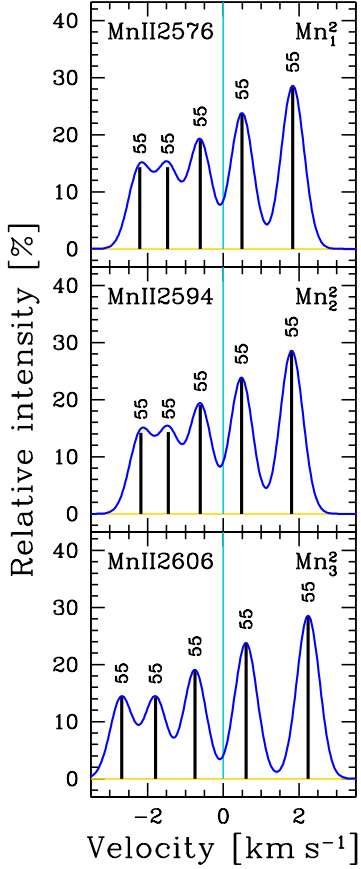
The  $q$  coefficients for Fe II in Table 9 were calculated using CI plus core–valence correlation corrections and Breit corrections in Porsev et al. (2007). On the other hand, the previous CI calculations by Dzuba et al. (2002) used experimental  $g$ -factors to model level pseudocrossing which, in some cases, can lead to larger corrections than core–valence correlations. Both sets of  $q$  values are consistent, and our recommended values are the simple average of the two. The transitions  $\lambda 2260$ ,  $\lambda 2249$ , and  $\lambda 2367$  were not calculated in those works: for these we use the values calculated using CI and experimental  $g$ -factor fitting presented in Berengut (2006), which shows good agreement with the other calculations for the other Fe II transitions.

## 2.12 Nickel

Table 10 provides the atomic data for the three Ni II transitions redwards of H I Ly $\alpha$  with precisely measured laboratory wavelengths. Several other similarly-strong Ni II transitions exist redwards of  $\sim 1370 \text{ \AA}$  but all with laboratory wavelength uncertainties significantly exceeding our  $\lesssim 20 \text{ m s}^{-1}$  criterion for varying  $\alpha$  studies. The three Ni II lines in Table 10 shift in the opposite direction to most transitions of other species as  $\alpha$  varies (i.e.  $q$  is negative), making them important lines to include in a multi-species fit of a quasar

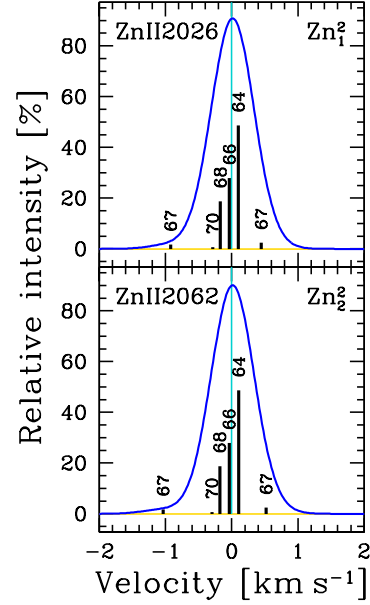
**Table 10.** Laboratory data for transitions of Ni of interest for quasar absorption-line varying- $\alpha$  studies described in Section 2.12. See Section 2.1 for full descriptions of each column.

Ion	Tran.	$A$	$\omega_0$ [cm <sup>-1</sup> ]	$X$	$\lambda_0$ [Å]	$\delta\nu$ [m s <sup>-1</sup> ]	Lower state	Upper state	ID	IP <sup>-</sup> , IP <sup>+</sup> [eV]	$f$ or %	$q$ [cm <sup>-1</sup> ]
Ni II	1709	58.6934	58493.0772(40) <sup>a,b</sup>	0	1709.60402(12)	20.5	3d <sup>9</sup> 2D <sub>5/2</sub>	3d <sup>8</sup> 4p z <sup>2</sup> F <sub>5/2</sub> <sup>o</sup>	Ni <sub>4</sub> <sup>2</sup>	7.64, 18.17	0.0324	-20 <sup>c</sup> (250)
	1741	58.6934	57420.0191(40) <sup>a,b</sup>	0	1741.55289(12)	20.9		3d <sup>8</sup> 4p z <sup>2</sup> D <sub>5/2</sub> <sup>o</sup>	Ni <sub>3</sub> <sup>2</sup>		0.0427	-1400 <sup>c</sup> (250)
	1751	58.6934	57080.3791(40) <sup>a,b</sup>	0	1751.91549(12)	21.0		3d <sup>8</sup> 4p z <sup>2</sup> F <sub>7/2</sub> <sup>o</sup>	Ni <sub>6</sub> <sup>2</sup>		0.0277	-700 <sup>c</sup> (250)

References: <sup>a</sup>Pickering et al. (2000); <sup>b</sup>Nave (2012); <sup>c</sup>Dzuba et al. (2002).**Figure 8.** Mn transition hyperfine structures in Table 8 described in Section 2.10. See Section 2.1 for Figure details.

absorber to constrain  $\alpha$ -variation. Also of note is the large range in  $q$ :  $\lambda 1709$  is effectively an “anchor” line, with a very small  $q$ , while  $\lambda 1741$  has a large, negative  $q$ . Therefore, like with Fe II, a single ionic species can, in principle, provide strong constraints on  $\alpha$ -variation. However, Ni has several stable isotopes, two of which have high relative abundances (<sup>58</sup>Ni and <sup>60</sup>Ni), and, to our knowledge, no isotopic structure measurements or calculations are available for the transitions in Table 10. That is, these Ni II transitions have unknown susceptibility to systematic effects related to isotopic abundance evolution.

The Ni II wavenumbers have been measured only once to high enough precision for varying  $\alpha$  studies by Pickering et al. (2000) using an FTS with an HCL. Their wavenumbers were calibrated using the older Ar II scale of Norlén (1973). Nave (2012) recommended increasing Pickering et al.’s wavenumbers by 10.6 parts in 10<sup>8</sup> to place them on the newer Whaling et al. (1995) Ar II calibration scale which is consistent with that of absolute standards derived from frequency comb measurements. The final composite

**Figure 10.** Zn transition isotopic and hyperfine structures in Table 11 described in Section 2.13. See Section 2.1 for Figure details.

wavenumbers shown in Table 10 are the values from Pickering et al. (2000) increased accordingly.

The recommended Ni II  $q$  coefficients in Table 10 are those calculated by Dzuba et al. (2002).

### 2.13 Zinc

Table 11 summarises the atomic data for Zn II  $\lambda\lambda 2026/2062$  fine-structure doublet and Fig. 7 illustrates the isotopic structures. No other Zn II transitions lying redwards of H I Lyman- $\alpha$  are known (Morton 2003). The Zn II doublet is particularly important in element abundance studies using quasar absorbers because Zn is expected to remain predominantly in the gas phase, having an apparently low affinity for condensing onto (or remaining condensed on) dust grains (Pettini et al. 1990). Nevertheless, these Zn II transitions are usually very weak because of the comparatively low abundance of Zn. Thus, even though the Zn II doublet has been used in some varying- $\alpha$  studies, it has generally not dominated the constraints (e.g. Murphy et al. 2001b; King et al. 2012). On the other hand, they are particularly sensitive to variations in  $\alpha$ , with  $\lambda 2026$  having the largest absolute  $q$  value of any transition considered in this paper.

The composite Zn II doublet wavenumbers have been measured with high enough precision in three separate analyses using FTSs with HCLs. The wavenumbers measured by Pickering et al. (2000) were calibrated using the older Ar II scale of Norlén (1973), while those measured by Aldenius et al. (2006) (see also



**Table 11.** Laboratory data for transitions of Zn of interest for quasar absorption-line varying- $\alpha$  studies described in Section 2.13. See Section 2.1 for full descriptions of each column.

Ion	Tran.	A	$\omega_0$ [cm <sup>-1</sup> ]	X	$\lambda_0$ [Å]	$\delta\nu$ [m s <sup>-1</sup> ]	Lower state	Upper state	ID	IP <sup>-</sup> , IP <sup>+</sup> [eV]	f or %	q [cm <sup>-1</sup> ]	
Zn II	2026	65.38	49355.00544(76) <sup>a,b,c,d</sup>	0	2026.136946(31)	4.6	3d <sup>10</sup> 4s <sup>2</sup> S <sub>1/2</sub>	3d <sup>10</sup> 4p <sup>2</sup> P <sub>3/2</sub> <sup>o</sup>	Zn <sub>1</sub> <sup>2</sup>	9.39, 17.96	0.501	2470 <sup>e,f</sup> (25)	
		70	49355.05268(86) <sup>g</sup>	2	2026.135007(35)	5.2						0.62%	
		68	49355.03373(80) <sup>g</sup>	2	2026.135785(33)	4.8						18.75%	
		67	49355.1572(50) <sup>h,g,i</sup>	3	2026.13072(21)	30.4	F = 2	F = 1, 2, 3				1.71%	
		67	49354.9316(18) <sup>h,g,i</sup>	3	2026.139979(76)	11.2	F = 3	F = 2, 3, 4				2.39%	
		66	49355.01138(79) <sup>g</sup>	2	2026.136702(32)	4.8						27.90%	
		64	49354.9888(10) <sup>g</sup>	2	2026.137628(43)	6.3						48.63%	
	2062	65.38	48481.08070(76) <sup>a,b,c,d</sup>	0	2062.660291(32)	4.7			3d <sup>10</sup> 4p <sup>2</sup> P <sub>1/2</sub> <sup>o</sup>	Zn <sub>2</sub> <sup>2</sup>		0.246	1563 <sup>e,f</sup> (25)
		70	48481.12899 <sup>j,g</sup>	3	2062.658236							0.62%	
		68	48481.10970 <sup>j,g</sup>	3	2062.659057							18.75%	
		67	48481.24812 <sup>h,j,g,i</sup>	3	2062.653167		F = 2	F = 2, 3				1.71%	
		67	48480.99644 <sup>h,j,g,i</sup>	3	2062.663876		F = 3	F = 2, 3				2.39%	
		66	48481.08685 <sup>j,g</sup>	3	2062.660029							27.90%	
		64	48481.06363 <sup>j,g</sup>	3	2062.661017							48.63%	

References: <sup>a</sup>Aldenius (2009); <sup>b</sup>Pickering et al. (2000); <sup>c</sup>Ruffoni & Pickering (2010); <sup>d</sup>Nave (2012); <sup>e</sup>Dzuba & Johnson (2007); <sup>f</sup>Savukov & Dzuba (2008); <sup>g</sup>Matsubara et al. (2003); <sup>h</sup>Campbell et al. (1997); <sup>i</sup>Dixit et al. (2008); <sup>j</sup>Berengut et al. (2003).

Aldenius 2009) were calibrated using the Whaling et al. (1995) scale. Nave (2012) placed both sets of measurements on a common calibration scale consistent with that of absolute standards derived from frequency comb measurements and we adopt Nave's corrections here. Ruffoni & Pickering (2010) also recently re-measured the Zn II transitions simultaneously with the Mg I/II and Ti II transitions discussed in Section 2.4 and Section 2.8. Their Ar II-calibrated Mg I wavenumbers agreed well with the frequency-comb based, absolute measurements of Hannemann et al. (2006) and Salumbides et al. (2006), and their Ti II  $\lambda\lambda$ 3067/3073 doublet wavenumbers agree with the corrected Aldenius (2009) values reported by Nave (2012). Therefore, we apply no correction to Ruffoni & Pickering's Zn II measurements. The final composite wavenumbers shown in Table 11 are a simple weighted mean of the corrected values from Pickering et al. (2000), Aldenius (2009) and the original values reported by Ruffoni & Pickering (2010).

Matsubara et al. (2003) have measured the isotopic separations in the  $\lambda$ 2026 transition between the most abundant isotope, <sup>64</sup>Zn, and <sup>66,68,70</sup>Zn using laser cooling and Fabry-Perot spectroscopic techniques. Laser cooling of <sup>67</sup>Zn was not possible in Matsubara et al.'s experiment, so we used equation (5) to estimate its isotopic shift,  $\delta\nu^{67,64}$ , with  $k_{\text{SMS}} \approx -1365(20)$  GHz.amu taken as a representative value from the measured  $\delta\nu^{68,66}$  in Matsubara et al.'s table 1, and multiplying the field shift  $F_{\text{FS}}\delta\langle r^2 \rangle^{66,64} = 0.35$  GHz by the scaling parameter  $\delta\langle r^2 \rangle^{67,66}/\delta\langle r^2 \rangle^{66,64} = 0.19$  from Campbell et al. (1997).

There does not appear to be any measurements of the Zn II  $\lambda$ 2062 isotopic separations, so we estimated them based on equation (5), the calculations of Berengut et al. (2003) and the measurements and calculations above for the  $\lambda$ 2026 line. For the  $\lambda$ 2062 specific mass shift constant ( $k_{\text{SMS}}$ ) we scaled the measured value for  $\lambda$ 2026 adopted above ( $-1365$  GHz.amu) by the ratio of the calculated values for  $\lambda$ 2062 and  $\lambda$ 2026 from Berengut et al. (i.e.  $-1310/-1266$ ). We assumed the field shift ( $F_{\text{FS}}$ ) for the  $\lambda$ 2062 transition was the same as that derived from measurements by Matsubara et al. (2003) for the  $\lambda$ 2026 transition, an assumption justified by the field shift estimates of Berengut et al. for the Zn II doublet.

The isotopic splittings illustrated in Fig. 10 are reasonably narrow. However, the terrestrial isotopic abundances being distributed fairly evenly amongst three of the isotopes (<sup>64,66,68</sup>Zn). Therefore, the systematic line-shifts induced by possible isotopic abundance

variations between quasar absorbers and the terrestrial environment could be appreciable. For example, Fenner et al. (2005) found that the dominant <sup>64</sup>Zn isotope in the terrestrial environment may have been even more abundant sub-dominant at the low metallicities typifying the highest column density quasar absorbers. This could lead to spurious line-shifts in both Zn II transitions of  $\sim 100$  m s<sup>-1</sup> (i.e. the separation between the <sup>64</sup>Zn II and composite transition velocities in Fig. 10).

To calculate the hyperfine splitting in the <sup>67</sup>Zn II  $\lambda\lambda$ 2026/2062 transitions we used equations (6)–(10) with the magnetic dipole and electric quadrupole hyperfine constants ( $A$  and  $B$ ) calculated for the ground and excited states by Dixit et al. (2008). Zn has a nuclear spin of  $I = 5/2$  so that the <sup>67</sup>Zn II  $\lambda$ 2026 ( $\lambda$ 2062) transition has 6 (4) allowed transitions, three (two) from each of the two ground states ( $F = 2$  and 3). The hyperfine splitting is dominated by that in the ground states so, as illustrated in Fig. 10, we represent the <sup>67</sup>Zn II  $\lambda\lambda$ 2026/2062 hyperfine structures with just two components each.

Figure 10 shows that the <sup>67</sup>Zn hyperfine splittings are quite large,  $\sim 1.5$  km s<sup>-1</sup>. This could cause substantial systematic effects in the measured line velocity if the isotopic abundance pattern – where <sup>67</sup>Zn comprises just 4.1% of Zn in the terrestrial environment (Rosman & Taylor 1998) – was very different in quasar absorbers. The expectation from the simulations of Fenner et al. (2005) is that <sup>67</sup>Zn should be even less abundant at the lower metallicities typical of the highest column density absorbers, but this is nevertheless a concern worth pointing out because there is currently no observational constraint on the Zn isotopic abundances in quasar absorbers.

Regarding the  $q$  coefficients in Table 11, most calculations treat Zn II as a single-valence-electron ion with a closed 3d<sup>10</sup> shell. While this is generally preferable to treating an 11 electron system with CI, it does make core–valence correlations large. Calculations of  $q$  coefficients including MBPT and the Breit interaction have been calculated by Dzuba et al. (2002) and Savukov & Dzuba (2008), and these are in excellent agreement. On the other hand, the coupled-cluster single–double method used in Dzuba & Johnson (2007) gives slightly different values. We have taken a simple average of the values from Dzuba & Johnson (2007) and Savukov & Dzuba (2008) in this case and assigned indicative errors in Table 11 which are large enough to accommodate both.

### 3 EFFECTS OF IGNORING ISOTOPIC/HYPERFINE STRUCTURE IN QUASAR ABSORPTION LINES

Some of the isotopic/hyperfine structures presented in Section 2, particularly for transitions of Mg I & II, Al III and Mn II, are broad and somewhat asymmetric (see Figs. 2, 3 & 8). Therefore, if those absorption lines are modelled using only their composite wavelengths, without the underlying isotopic/hyperfine structure, we can expect systematic errors in the fitted parameters – the redshifts (or velocities), column densities and Doppler parameters. We explore these systematic effects below.

#### 3.1 Velocity shifts

For varying- $\alpha$  studies, systematic effects on the fitted redshifts (or velocities) of absorption lines are particularly important. If absorption lines with underlying structure are fitted with just a single component, velocity shifts will be measured which may be attributed to a varying  $\alpha$ , or at least contribute important systematic errors to varying- $\alpha$  measurements.

To explore the magnitude and sign of these spurious velocity shifts as a function of the strength of the absorption lines, we created synthetic, high signal-to-noise ratio ( $S/N = 10^5$  per pixel) spectra with resolving power  $R = 75000$  and dispersion  $1.3 \text{ km s}^{-1}$  containing a single velocity component of all the transitions studied in this paper and including the isotopic/hyperfine structures illustrated in Figs. 2–10. The Doppler broadening parameter was set to  $b = 2.5 \text{ km s}^{-1}$  for all ionic species. The relative column densities of the different singly-ionized species were assumed to follow the meteoritic solar abundance pattern of Asplund et al. (2009, table 1). To obtain representative column densities for the sub-dominant ions, Mg I, Al III and Si IV, we assumed the median observed values of  $\log[N(\text{Mg I})/N(\text{Mg II})] = -1.8$  by Churchill & Vogt (2001),  $\log[N(\text{Al III})/N(\text{Al II})] = -0.6$  and  $\log[N(\text{Si IV})/N(\text{Si II})] = -1.0$  by Prochaska et al. (2002). Representative column density ratios for the sub-dominant ions Na I and Ca II are much more difficult to estimate because they vary strongly according to the local absorber conditions, especially the dust content of the gas. Here we adopt the following rough values for illustration purposes only, guided by the few available measurements of  $\log[N(\text{Na I})/N(\text{Ca II})]$  and photoionization modelling conducted by Richter et al. (2011):  $\log[N(\text{Na I})/N(\text{Ca II})] = -0.6$  and  $\log[N(\text{Ca II})/N(\text{Mg II})] = -1.2$ .

We created synthetic spectra with a range of Fe II column densities, scaling the other species' column densities appropriately, and fitted them using only the composite transition wavelengths shown in Tables 1–11. The fits were performed using the non-linear least squares code `VPFIT`<sup>4</sup> which was designed for, and has been used in, numerous quasar absorption line studies, including most previous varying- $\alpha$  analyses.

Figure 11 shows the velocity shift caused by ignoring the underlying isotopic/hyperfine structure of a single quasar absorption line. Clearly, the largest systematic effects occur in high column density absorption lines of Na I, Mg II, Al III and Mn II. For example, at a Mg II column density of  $\log[N(\text{Mg II})/\text{cm}^{-2}] - 0.08 = \log[N(\text{Fe II})/\text{cm}^{-2}] \sim 15.5$ , a spurious velocity shift of  $\sim -20 \text{ m s}^{-1}$  will be measured in the Mg II doublet transitions, while the broad and asymmetric hyperfine structures of the Al III doublet and Mn II triplet lead to velocity shifts of  $\sim -120$  and  $\sim -30 \text{ m s}^{-1}$  respectively. The reason for the strong dependence of velocity shift on

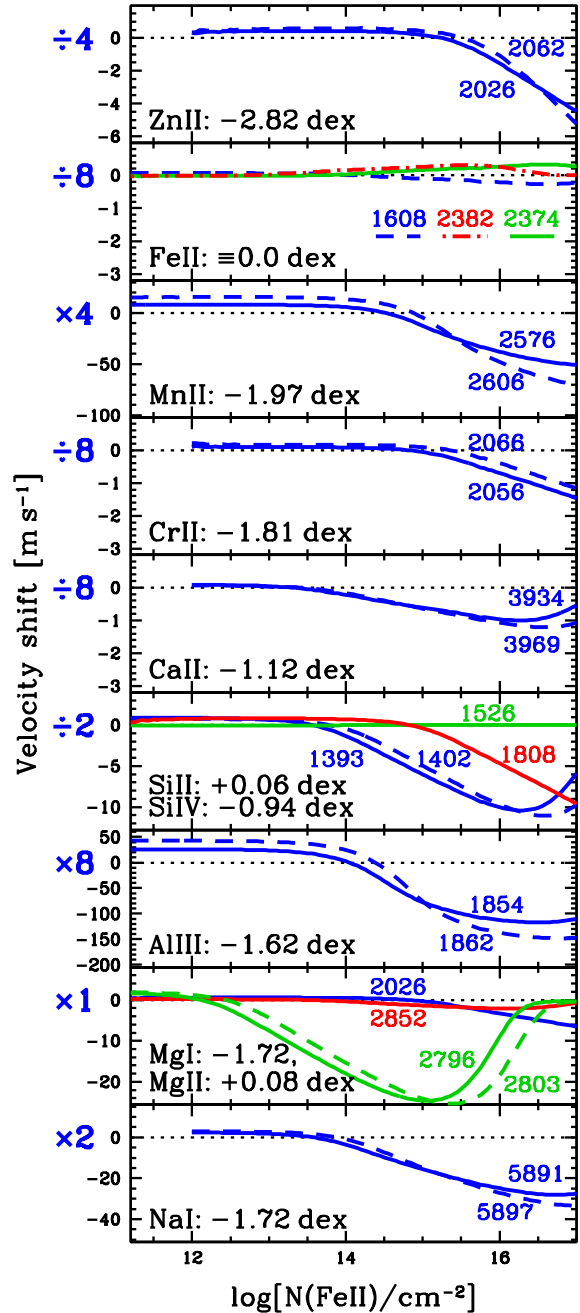


**Figure 11.** Spurious velocity shift derived from fitting synthetic absorption line spectra without taking into account the underlying isotopic/hyperfine structures. Selected ionic species are represented in different panels, with each line representing a different transition (labelled with its transition wavelength in Å). The column density of each ionic species, relative to that of Fe II, assumed in the simulated spectra is provided in each panel. The vertical scale of each panel varies; as a quick guide, the factor by which it differs to that of the Mg panel (bottom panel), is provided at the left of each panel.

the absorption line strength [parametrized by  $N(\text{Fe II})$ ] is due to ‘differential isotopic saturation’ (Murphy et al. 2001a): as the column density increases and the strongest isotopic component of the absorption line saturates, the relative influence of the weaker components increases, shifting the line centroid towards the simple mean of the isotopic component velocities. For the strongest

<sup>4</sup> <http://www.ast.cam.ac.uk/~rfc/vpfit.html>.

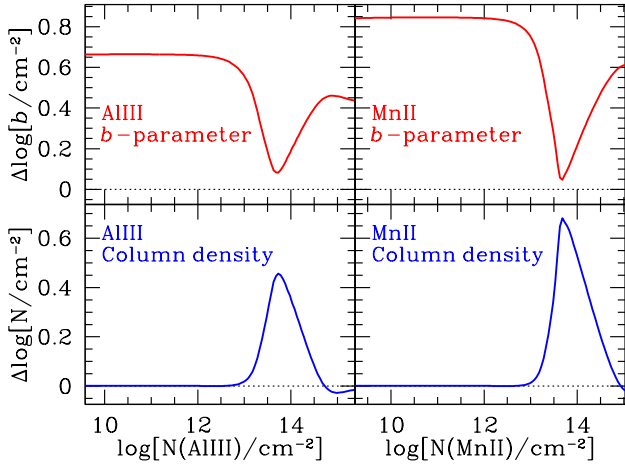


**Figure 12.** Systematic errors in the column densities and Doppler  $b$ -parameters of Al III and Mn II derived from simulations with an input  $b = 2.5 \text{ km s}^{-1}$ . The simulations were created with the prominent hyperfine structures of the Al III and Mn II shown in Figs. 3 and 2 but were fitted with a model lacking that underlying structure.

transitions, particularly the Mg II doublet, this trend is overcome and reversed with even higher column density. This is because the damping wings of the strongest isotopic components begin to dominate the profile shape, moving the fitted centroid back towards the component-strength-weighted mean velocity.

Finally, it is also evident in Fig. 11 that, for some transitions, there is a small non-zero velocity shift even at very low column densities, when the absorption line is optically thin. This is due to the small non-Voigt shape of the absorption line introduced by the underlying isotopic/hyperfine components. Thus, it is largest in transitions of Al III and Mn II which have the most extreme hyperfine structures studied here.

### 3.2 Column densities and Doppler $b$ -parameters

Figure 12 shows the systematic effect on the fitted column density ( $N$ ) and Doppler broadening parameters ( $b$ ) of Al III and Mn II when the very pronounced hyperfine structures of their transitions are ignored (see Figs. 3 and 8). The same simulations and fitting approach used to derive the spurious velocity shifts in Section 3.1 were used here. Clearly, the systematic effects on  $N$  and  $b$  are anti-correlated, as expected if the fit is to recover approximately the correct equivalent width of absorption in each transition. However, it is important to recognise that, at low  $N$  values where the transitions are optically thin (i.e.  $\log[N/\text{cm}^{-2}] \lesssim 13$ ), the systematic effect on  $N$  is negligible while that on  $b$  is a maximum and  $\sim 0.7 \text{ km s}^{-1}$ . The opposite is true when the transitions are saturated, with the effect on  $b$  reducing considerably to only  $\sim 0.2 \text{ km s}^{-1}$  but that on  $N$  increasing to  $\sim 0.4\text{--}0.6$  dex, or column density overestimates by factors of  $\sim 2.5\text{--}4$ . However, for saturated transitions at more realistic  $S/N$  values of  $\sim 15\text{--}50$  per pixel (cf.  $10^5$  in the simulations for Fig. 12), the statistical uncertainty on the column density is very large and altogether unreliable.

Thus, of the  $b$  parameters and column densities, the former are most affected in practical sense by ignoring the hyperfine structures is the systematic error on  $b$  for optically thin lines. In varying- $\alpha$  studies, this will manifest itself as an inability to simultaneously fit the Al III and Mn II with other species with much narrower or no isotopic/hyperfine structures: linking the  $b$  parameters between

species in the fit may yield poor (i.e. statistically unacceptable or unlikely) fits to some/all transitions.

## 4 CONCLUSIONS

We have reviewed and synthesized the existing laboratory atomic data for metal-line transitions with precisely-known frequencies ( $\delta\nu \lesssim 20 \text{ m s}^{-1}$ ). These transitions are of particular interest for quasar absorption-line studies of possible cosmological variations in the fine-structure constant,  $\alpha$ , where the primary concern is the accuracy of the laboratory frequency and knowledge about any significant isotopic and/or hyperfine structure. For all transitions presented here, the composite frequencies should be accurate to within the stated uncertainties, as should the isotopic/hyperfine frequencies in transitions where those quantities are measured directly (Na I, Mg I & II, Al III, Ca II, Mn II and Zn II  $\lambda 2026$ ). However, for most transitions – those of Si II & IV, Ti II, Cr II, Fe II and Zn II  $\lambda 2062$  – the isotopic/hyperfine splittings are calculated, typically with *ab initio* techniques. Indeed, we presented new isotopic structure calculations of this sort for the Si II and Ti II transitions, including Si II  $\lambda 1808$  and Ti II  $\lambda \lambda 1910.6/1910.9$  for the first time, and found close agreement with previous estimates for the other transitions. Nevertheless, it is difficult to estimate how closely any calculated isotopic structures reflect the real ones; isotopic structure *measurements* for these transitions are encouraged. Finally, note that we have no current information about the isotopic structures of Fe II  $\lambda 2260$  and the Ni II transitions of interest.

Independent, repeated laboratory frequency measurements are critical for ensuring that tests of the invariance of the fundamental constants over cosmological time- and distance-scales are reliable. Most transitions studied here have multiple laboratory frequency measurements which, following the re-calibration work of Nave & Sansonetti (2011) and Nave (2012), agree within the uncertainties. The exceptions to this are the transitions measured by Griesmann & Kling (2000) (i.e. Al II & III and Si II & IV), the bluest and reddest Ti II transitions ( $\lambda 1910.6$ ,  $1910.9$ ,  $3230$ ,  $3242$  and  $3384$ ), some relatively weak, though nevertheless important, Fe II transitions ( $\lambda 1608$ ,  $1611$ ,  $2249$  and  $2367$ ), and the Ni II lines. All the transitions presented here are calibrated on frequency scales that are consistent with the absolute and highly-accurate one derived in frequency comb measurements. The accuracy of the frequencies for many transitions relies on the Ar II calibration scale of Whaling et al. (1995) (which is consistent with frequency comb measurements). However, for the far-UV, Ar II-calibrated transitions without independent, repeated measurements (e.g. those of Griesmann & Kling 2000), Nave (2012) cautions that extending the calibration far into the UV with confidence is difficult.

Table 12 summarizes the most important missing information for the ions considered in this paper. It includes the transitions in Tables 1–11 for which repeated laboratory frequency measurements are desirable and/or we have no current information (measurement or calculation) about their isotopic structures. This table also includes ions which did not qualify to appear in Tables 1–11, either because the laboratory frequency has not been measured with  $\delta\nu \lesssim 20 \text{ m s}^{-1}$  accuracy and/or the  $q$  coefficient is not known (to our knowledge). Missing information which prevents ions not considered in this paper from being useful in varying- $\alpha$  studies is summarized in Berengut et al. (2011).

Given the now rather complete, if not completely certain, isotopic/hyperfine structure information for most transitions studied here, we were able to explore the likely systematic errors incurred

**Table 12.** Summary of the most important missing information for the ions discussed in this paper. For other ions, see Berengut et al. (2011). The “Missing” column specifies the new measurements/calculations that are either required before the transition can be used in varying- $\alpha$  analyses (underlined) or desirable to improve the reliability of such work (not underlined). In particular, the transitions from Tables 1–11 for which repeated laboratory measurements do not exist are included here.

Ion	Tran.	$\omega_0$ [cm <sup>-1</sup> ]	$\lambda_0$ [Å]	ID	Missing <sup>a</sup>
Al II	1670	59851.976(4) <sup>b</sup>	1670.78861(11)	Al <sub>1</sub> <sup>2</sup>	$\omega$
Al III	1854	53916.5480(11) <sup>b</sup>	1854.718146(39)	Al <sub>1</sub> <sup>3</sup>	$\omega$
	1862	53682.8884(11) <sup>b</sup>	1862.790974(39)	Al <sub>2</sub> <sup>3</sup>	$\omega$
Si II	1260	79338.50 <sup>c</sup>	1260.4221	Si <sub>1</sub> <sup>2</sup>	$\omega$
	1304	76665.35 <sup>c</sup>	1304.3702	Si <sub>3</sub> <sup>2</sup>	$\omega$
	1526	65500.4538(7) <sup>b</sup>	1526.706980(16)	Si <sub>2</sub> <sup>2</sup>	$\omega$
	1808	55309.3404(4) <sup>b</sup>	1808.012883(13)	Si <sub>4</sub> <sup>2</sup>	$\omega$
Si IV	1393	71748.355(2) <sup>b</sup>	1393.760177(39)	Si <sub>1</sub> <sup>4</sup>	$\omega$
	1402	71287.376(2) <sup>b</sup>	1402.772912(39)	Si <sub>2</sub> <sup>4</sup>	$\omega$
Ti II	1910.6	52339.240(1) <sup>d</sup>	1910.61238(4)	Ti <sub>2</sub> <sup>2</sup>	$\omega$
	1910.9	52329.889(1) <sup>d</sup>	1910.95380(4)	Ti <sub>2</sub> <sup>2</sup>	$\omega$
	3230	30958.5871(10) <sup>e,f</sup>	3230.12157(10)	Ti <sub>6</sub> <sup>2</sup>	$\omega$
	3242	30836.4271(10) <sup>e,f</sup>	3242.91785(11)	Ti <sub>2</sub> <sup>2</sup>	$\omega$
	3384	29544.4551(10) <sup>e,f</sup>	3384.72988(11)	Ti <sub>2</sub> <sup>2</sup>	$\omega$
Fe I	2167	46137.098(1) <sup>g,h</sup>	2167.4532(5)	Fe <sub>1</sub> <sup>1</sup>	$\omega, q$
	2298	43499.506(6) <sup>g,h</sup>	2298.8767(3)	Fe <sub>11</sub> <sup>1</sup>	$\omega, q$
	2463	40594.432(5) <sup>g,h</sup>	2463.3920(3)	Fe <sub>6</sub> <sup>1</sup>	$\omega$
	2484	40257.313(10) <sup>g,h</sup>	2484.0207(6)	Fe <sub>1</sub> <sup>1</sup>	$\omega$
	2501	39969.852(5) <sup>g,h</sup>	2501.8857(3)	Fe <sub>7</sub> <sup>1</sup>	$\omega, I$
	2523	39625.804(5) <sup>g,h</sup>	2523.6081(3)	Fe <sub>2</sub> <sup>1</sup>	$\omega$
	2719	36766.966(5) <sup>g,h</sup>	2719.8328(4)	Fe <sub>4</sub> <sup>1</sup>	$\omega$
	2967	33695.397(5) <sup>g,h</sup>	2967.7644(4)	Fe <sub>8</sub> <sup>1</sup>	$\omega$
	2984	33507.124(4) <sup>g,h</sup>	2984.4400(4)	Fe <sub>10</sub> <sup>1</sup>	$\omega$
	3021	33095.942(5) <sup>g,h</sup>	3021.5185(5)	Fe <sub>5</sub> <sup>1</sup>	$\omega$
	3441	29056.323(5) <sup>g,h</sup>	3441.5917(6)	Fe <sub>12</sub> <sup>1</sup>	$\omega, \Gamma$
	3720	26874.550(5) <sup>g,h</sup>	3720.9926(7)	Fe <sub>9</sub> <sup>1</sup>	$\omega$
	3861	25899.989(5) <sup>g,h</sup>	3861.0055(7)	Fe <sub>13</sub> <sup>1</sup>	$\omega$
Fe II	1260	79331.359(4) <sup>f</sup>	1260.53557(6)	Fe <sub>7</sub> <sup>2</sup>	$\omega, q$
	1588	62945.045(2) <sup>i</sup>	1588.68741(6)	Fe <sub>11</sub> <sup>2</sup>	$\omega, q$
	1608	62171.623(3) <sup>f</sup>	1608.450852(78)	Fe <sub>5</sub> <sup>2</sup>	$\omega$
	1611	62065.527(3) <sup>f</sup>	1611.200369(78)	Fe <sub>10</sub> <sup>2</sup>	$\omega$
	1620	61726.069(3) <sup>i</sup>	1620.06106(7)	Fe <sub>13</sub> <sup>2</sup>	$\omega, q$
	1901	52582.850(2) <sup>i</sup>	1901.76075(9)	Fe <sub>12</sub> <sup>2</sup>	$\omega, q$
	2234	44753.818(2) <sup>i</sup>	2234.44624(9)	Fe <sub>14</sub> <sup>2</sup>	$\omega, q$
	2249	44446.9044(19) <sup>f</sup>	2249.875472(96)	Fe <sub>9</sub> <sup>2</sup>	$\omega$
	2260	44232.5390(19) <sup>e,f</sup>	2260.779108(97)	Fe <sub>8</sub> <sup>2</sup>	$I$
	2367	42237.0563(19) <sup>f</sup>	2367.58924(11)	Fe <sub>15</sub> <sup>2</sup>	$\omega$
Ni II	1317	75917.64 <sup>c</sup>	1317.217	Ni <sub>2</sub> <sup>2</sup>	$\omega, I$
	1370	72985.67 <sup>c</sup>	1370.132	Ni <sub>1</sub> <sup>2</sup>	$\omega, I$
	1393	71770.82 <sup>c</sup>	1393.324	Ni <sub>7</sub> <sup>2</sup>	$\omega, f, I$
	1454	68735.99 <sup>c</sup>	1454.842	Ni <sub>5</sub> <sup>2</sup>	$\omega, I$
	1467.2	68154.31 <sup>c</sup>	1467.259	Ni <sub>9</sub> <sup>2</sup>	$\omega, I$
	1467.7	68131.21 <sup>c</sup>	1467.756	Ni <sub>2</sub> <sup>2</sup>	$\omega, I$
	1502	66571.34 <sup>c</sup>	1502.148	Ni <sub>11</sub> <sup>2</sup>	$\omega, f, I$
	1703	58705.713(15) <sup>j,f</sup>	1703.41172(44)	Ni <sub>10</sub> <sup>2</sup>	$\omega, I$
	1709	58493.0772(40) <sup>j,f</sup>	1709.60402(12)	Ni <sub>4</sub> <sup>2</sup>	$\omega, I$
	1741	57420.0191(40) <sup>j,f</sup>	1741.55289(12)	Ni <sub>2</sub> <sup>2</sup>	$\omega, I$
	1751	57080.3791(40) <sup>j,f</sup>	1751.91549(12)	Ni <sub>6</sub> <sup>2</sup>	$\omega, I$

<sup>a</sup>Key for “missing” information:  $\omega$  = frequency meas.;  $q$  =  $q$  coefficient calc.;  $f$  = oscillator strength meas./calc.;  $\Gamma$  = damping constant meas./calc.;  $I$  = isotopic structure meas./calc.

References: <sup>b</sup>Griesmann & Kling (2000); <sup>c</sup>Morton (2003); <sup>d</sup>Ruffoni & Pickering (2010); <sup>e</sup>Aldenius (2009); <sup>f</sup>Nave (2012); <sup>g</sup>Nave et al. (1994); <sup>h</sup>Nave & Sansonetti (2011); <sup>i</sup>Nave & Johansson (2013); <sup>j</sup>Pickering et al. (2000).

in quasar absorption-line analyses if these structures are ignored. For example, differential saturation of the Mg isotopic components will cause spurious line-shifts of up to  $\sim 20$  m s<sup>-1</sup> in the strong and often-used Mg II doublet transitions if the isotopic structure is not modelled. The same effect in the broadly-spaced hyperfine structures of the Al III and Mn II transitions is much more pronounced, particularly for the former, causing spurious shifts of up to  $\sim 120$  m s<sup>-1</sup>. We also find that the Doppler broadening parameters ( $b$ ) for the Al III and Mn II transitions will be systematically overestimated by  $\sim 0.6$  and  $\sim 0.8$  km s<sup>-1</sup>, respectively, in the optically thin regime if the hyperfine structures are not taken into account. However, the column density estimates will be almost unaffected in such cases, assuming that more than one transition of each species is measured simultaneously and the velocity structure of the absorption is simple and well-resolved. These latter conditions are often not met in real quasar absorption analyses. For varying- $\alpha$  analyses, in which accurate absorption profile modelling is required, ignoring the Al III and Mn II hyperfine structures causes substantial difficulties in fitting these transitions simultaneously with those of other species, undermining the assumptions and reliability of the many-multiplet method.

Finally, to ensure the transparency, repeatability and ease of updating the laboratory data and isotopic/hyperfine structure calculations presented here, we supply a spreadsheet containing all data details and calculations in the Supporting Information. This will be maintained and updated at <https://researchdata.and.s.org.au/laboratory-atomic-transition-data-for-precise-optical-quasar-absorption-spectroscopy> and readers are invited to alert the authors to updated information and/or to request that new transitions be included.

## ACKNOWLEDGMENTS

The authors thank the Australian Research Council for *Discovery Project* grant DP110100866 which supported this work. Part of this research was undertaken on the NCI National Facility, which is supported by the Australian Commonwealth Government.

## REFERENCES

- Aldenius M., 2009, *Phys. Scr.*, 134, 014008  
Aldenius M., Johansson S., Murphy M.T., 2006, *MNRAS*, 370, 444  
Angeli I., 2004, *At. Data Nucl. Data Tables*, 87, 185  
Angstmann E.J., Dzuba V.A., Flambaum V.V., 2004, *Phys. Rev. A*, 70, 014102  
Arbes F., Benzing M., Gudjons T., Kurth F., Werth G., 1994, *Z. Phys. D*, 31, 27  
Ashenfelter T., Mathews G.J., Olive K.A., 2004, *Phys. Rev. Lett.*, 92, 041102  
Asplund M., Grevesse N., Sauval A.J., Scott P., 2009, *ARA&A*, 47, 481  
Bahcall J.N., Salpeter E.E., 1965, *ApJ*, 142, 1677  
Balling P., Kfen P., 2008, *Eur. Phys. J. D*, 48, 3  
Batteiger V. et al., 2009, *Phys. Rev. A*, 80, 022503  
Beckmann A., Böklen K.D., Elke D., 1974, *Z. Phys.*, 270, 173  
Berengut J.C., 2006, PhD thesis, Univ. New South Wales  
Berengut J.C., 2011, *Phys. Rev. A*, 84, 052520  
Berengut J.C., Dzuba V.A., Flambaum V.V., 2003, *Phys. Rev. A*, 68, 022502  
Berengut J.C., Dzuba V.A., Flambaum V.V., King J.A., Kozlov M.G., Murphy M.T., Webb J.K., 2011, *Atomic Transition Frequencies, Isotope Shifts, and Sensitivity to Variation of the Fine Structure Constant for Studies of Quasar Absorption Spectra*, Martins C., Molaro

- P., eds., *Astrophys. Space Sci. Proc.*, Springer, Berlin Heidelberg, p.9, arXiv:1011.4136
- Berengut J.C., Dzuba V.A., Flambaum V.V., Marchenko M.V., 2004, *Phys. Rev. A*, 70, 064101
- Berengut J.C., Flambaum V.V., Kozlov M.G., 2005, *Phys. Rev. A*, 72, 044501
- Berengut J.C., Flambaum V.V., Kozlov M.G., 2006, *Phys. Rev. A*, 73, 012504
- Berengut J.C., Flambaum V.V., Kozlov M.G., 2008, *J. Phys. B*, 41, 235702
- Blackwell-Whitehead R.J., Toner A., Hibbert A., Webb J., Ivarsson S., 2005, *MNRAS*, 364, 705
- Bouché N., Murphy M.T., Kacprzak G.G., Péroux C., Contini T., Martin C.L., Dessauges-Zavadsky M., 2013, *Science*, 341, 50
- Campbell P., Billowes J., Grant I.S., 1997, *J. Phys. B*, 30, 2351
- Churchill C.W., Vogt S.S., 2001, *AJ*, 122, 679
- Cowie L.L., Songaila A., 1995, *ApJ*, 453, 596
- Dessauges-Zavadsky M., Calura F., Prochaska J.X., D'Odorico S., Matteucci F., 2007, *A&A*, 470, 431
- Dixit G., Nataraj H.S., Sahoo B.K., Chaudhuri R.K., Majumder S., 2008, *J. Phys. B*, 41, 025001
- Dzuba V.A., Flambaum V.V., 2008, *Phys. Rev. A*, 77, 012514
- Dzuba V.A., Flambaum V.V., Kozlov M.G., 1996, *Phys. Rev. A*, 54, 3948
- Dzuba V.A., Flambaum V.V., Kozlov M.G., Marchenko M., 2002, *Phys. Rev. A*, 66, 022501
- Dzuba V.A., Flambaum V.V., Webb J.K., 1999a, *Phys. Rev. A*, 59, 230
- Dzuba V.A., Flambaum V.V., Webb J.K., 1999b, *Phys. Rev. Lett.*, 82, 888
- Dzuba V.A., Johnson W.R., 2007, *Phys. Rev. A*, 76, 062510
- Fenner Y., Murphy M.T., Gibson B.K., 2005, *MNRAS*, 358, 468
- Griesmann U., Kling R., 2000, *ApJL*, 536, L113
- Gunn J.E., Peterson B.A., 1965, *ApJ*, 142, 1633
- Hannemann S., Salumbides E.J., Witte S., Zinkstok R.T., van Duijn E.-J., Eikema K. S.E., Ubachs W., 2006, *Phys. Rev. A*, 74, 012505
- Itano W.M., Wineland D.J., 1981, *Phys. Rev. A*, 24, 1364
- Jomaron W.R., Sapirstein J., 1986, *Phys. Rev. Lett.*, 57, 1126
- Jomaron C.M., Dworetzky M.M., Allen C.S., 1999, *MNRAS*, 303, 555
- Juncar P., Pinard J., Hamon J., Chartier A., 1981, *Metrologia*, 17, 77
- King J.A., Webb J.K., Murphy M.T., Flambaum V.V., Carswell R.F., Bainbridge M.B., Wilczynska M.R., Koch F.E., 2012, *MNRAS*, 422, 3370
- Kozlov M.G., Korol V.A., Berengut J.C., Dzuba V.A., Flambaum V.V., 2004, *Phys. Rev. A*, 70, 062108
- Kozlov M.G., Porsev S.G., 1999, *Opt. Spectrosc.*, 87, 352
- Levshakov S.A., Centurión M., Molaro P., Kostina M.V., 2006, *A&A*, 447, L21
- Lu L., Wolfe A.M., Turnshek D.A., Lanzetta K.M., 1993, *ApJS*, 84, 1
- Maleki S., Goble A.T., 1992, *Phys. Rev. A*, 45, 524
- Mårtensson-Pendrill A.-M. et al., 1992, *Phys. Rev. A*, 45, 4675
- Matsubara K., Tanaka U., Imajo H., Urabe S., Watanabe M., 2003, *App. Phys. B*, 76, 209
- Molaro P. et al., 2013, *A&A*, 555, A68
- Molaro P., Reimers D., Agafonova I.I., Levshakov S.A., 2008, *Eur. Phys. J. Special Topics*, 163, 173
- Morton D.C., 1991, *ApJS*, 77, 119
- Morton D.C., 2003, *ApJS*, 149, 205
- Murphy M.T., Webb J.K., Flambaum V.V., 2003, *MNRAS*, 345, 609
- Murphy M.T., Webb J.K., Flambaum V.V., Churchill C.W., Prochaska J.X., 2001a, *MNRAS*, 327, 1223
- Murphy M.T., Webb J.K., Flambaum V.V., Dzuba V.A., Churchill C.W., Prochaska J.X., Barrow J.D., Wolfe A.M., 2001b, *MNRAS*, 327, 1208
- Murphy M.T., Webb J.K., Flambaum V.V., Prochaska J.X., Wolfe A.M., 2001c, *MNRAS*, 327, 1237
- Nave G., 2012, *MNRAS*, 420, 1570
- Nave G., Johansson S., 2013, *ApJS*, 204, 1
- Nave G., Johansson S., Learner R. C.M., Thorne A.P., Brault J.W., 1994, *ApJS*, 94, 221
- Nave G., Sansonetti C.J., 2011, *J. Opt. Soc. Am. B*, 28, 737
- Norlén G., 1973, *Phys. Scr.*, 8, 249
- Nörtershäuser W., Blaum K., Icker K., Müller P., Schmitt A., Wendt K., Wiche B., 1998, *Eur. Phys. J. D*, 2, 33
- Pettini M., Boksenberg A., Hunstead R.W., 1990, *ApJ*, 348, 48
- Pickering J.C., Thorne A.P., Murray J.E., Litzén U., Johansson S., Zilio V., Webb J.K., 2000, *MNRAS*, 319, 163
- Pickering J.C., Thorne A.P., Webb J.K., 1998, *MNRAS*, 300, 131
- Porsev S.G., Koshelev K.V., Tupitsyn I.I., Kozlov M.G., Reimers D., Levshakov S.A., 2007, *Phys. Rev. A*, 76, 052507
- Porsev S.G., Kozlov M.G., Reimers D., 2009, *Phys. Rev. A*, 79, 032519
- Prochaska J.X., Chen H.-W., Wolfe A.M., Dessauges-Zavadsky M., Bloom J.S., 2008, *ApJ*, 672, 59
- Prochaska J.X., Henry R. B.C., O'Meara J.M., Tytler D., Wolfe A.M., Kirkman D., Lubin D., Suzuki N., 2002, *PASP*, 114, 933
- Prochaska J.X., McWilliam A., 2000, *ApJ*, 537, L57
- Prochaska J.X., Wolfe A.M., 1996, *ApJ*, 470, 403
- Rauch M., 1998, *ARA&A*, 36, 267
- Richter P., Krause F., Fechner C., Charlton J.C., Murphy M.T., 2011, *A&A*, 528, A12
- Rosman K. J.R., Taylor P. D.P., 1998, *J. Phys. Chem. Ref. Data*, 27, 1275
- Ruffoni M.P., Pickering J.C., 2010, *ApJ*, 725, 424
- Safronova M.S., Johnson W.R., 2001, *Phys. Rev. A*, 64, 052501
- Salumbides E.J., Hannemann S., Eikema K. S.E., Ubachs W., 2006, *MNRAS*, 373, L41
- Savedoff M.P., 1956, *Nature*, 178, 688
- Savukov I.M., Dzuba V.A., 2008, *Phys. Rev. A*, 77, 042501
- Schmidt M., 1963, *Nature*, 197, 1040
- Sur C., Sahoo B.K., Chaudhuri R.K., Das B.P., Mukherjee D., 2005, *Eur. Phys. J. D*, 32, 25
- Tupitsyn I.I., Shabaev V.M., López-Urrutia J. R.C., Draganić I., Orts R.S., Ullrich J., 2003, *Phys. Rev. A*, 68, 022511
- van Wijngaarden W.A., Li J., 1994, *Z. Phys. D*, 32, 67
- Varshalovich D.A., Panchuk V.E., Ivanchik A.V., 1996, *Astron. Lett.*, 22, 6
- Webb J.K., Flambaum V.V., Churchill C.W., Drinkwater M.J., Barrow J.D., 1999, *Phys. Rev. Lett.*, 82, 884
- Webb J.K., King J.A., Murphy M.T., Flambaum V.V., Carswell R.F., Bainbridge M.B., 2011, *Phys. Rev. Lett.*, 107, 191101
- Webb J.K., Murphy M.T., Flambaum V.V., Dzuba V.A., Barrow J.D., Churchill C.W., Prochaska J.X., Wolfe A.M., 2001, *Phys. Rev. Lett.*, 87, 091301
- Whaling W., Anderson W. H.C., Carle M.T., Brault J.W., Zarem H.A., 1995, *J. Quant. Spectrosc. Radiat. Transfer*, 53, 1
- Wolf A.L., van den Berg S.A., Gohle C., Salumbides E.J., Ubachs W., Eikema K. S.E., 2008, *Phys. Rev. A*, 78, 032511
- Wolf A.L., van den Berg S.A., Ubachs W., Eikema K. S.E., 2009, *Phys. Rev. Lett.*, 102, 223901
- Wolfe A.M., Gawiser E., Prochaska J.X., 2005, *ARA&A*, 43, 861
- Yei W., Bierdzan A., Havey M.D., 1993, *Phys. Rev. A*, 48, 1909
- Zych B.J., Murphy M.T., Hewett P.C., Prochaska J.X., 2009, *MNRAS*, 392, 1429

## APPENDIX A: NEW ATOMIC CALCULATIONS FOR SINGLY-IONISED SILICON AND TITANIUM

New *ab initio* calculations of the  $q$ -values and isotope shifts presented for Si II and Ti II were performed using the atomic structure package AMBiT, an implementation of the combination of configuration interaction and many-body perturbation theory (CI+MBPT) described in Berengut et al. (2006) (see also Dzuba et al. 1996; Berengut et al. 2005). Both Si II and Ti II are well-approximated as three-valence-electron ions above a closed-shell core. The calculations closely follow the strategy adopted for Ti II in Berengut et al. (2008).

Briefly, the calculations start by solving the Dirac-Fock (relativistic Hartree-Fock) equations to obtain single-particle orbitals for the core electrons, which are frozen at CI level. We then diagonalize the Dirac-Fock Hamiltonian over a set of 40 b-splines (Johnson & Sapirstein 1986) spanning 40 atomic units to obtain a large

set of valence and virtual orbitals from which we select those with the lowest eigenvalues. In this work we use a basis size 16spdf for the configuration interaction, indicating that states 1s–16s, 2p–16p, etc., are included. This is enough to saturate the CI energy levels in Si II and Ti II.

Valence-valence correlations are treated to all orders by the configuration interaction. Core-valence correlations, that go beyond the frozen-core approximation, are treated using MBPT to second order of the residual Coulomb interaction by modifying the radial integrals in the CI procedure. The MBPT basis can be made somewhat larger than the CI basis, which allows for saturation of the effect of virtual excitations from the closed-shell core (to second order). The MBPT operator may be separated into one-, two-, and three-valence electron parts, denoted  $\Sigma^{(1)}$ ,  $\Sigma^{(2)}$ , and  $\Sigma^{(3)}$ . It was shown by Berengut et al. (2008) that the effective three-body operator,  $\Sigma^{(3)}$ , is important for isotope shift calculations in Ti II, and in this work we also include it in our Si II calculations, although it plays a smaller role in this system.

The fine-structure constant,  $\alpha$ , is a free parameter in AMBiT that must be entered by hand. To obtain the sensitivity of transitions to  $\alpha$ -variation,  $q$ , the entire spectrum is recalculated with smaller and larger values of  $\alpha$ .  $q$  is then the numerical derivative at  $\alpha_0$ , the current value of  $\alpha$ :

$$q = \left. \frac{d\omega}{d\alpha^2} \right|_{\alpha=\alpha_0}.$$

The specific mass shift,  $k_{\text{SMS}}$ , is obtained from AMBiT using the finite-field method of Berengut et al. (2003). The SMS is a two-body operator, proportional to  $\vec{p}_1 \cdot \vec{p}_2$ , and it is added to the Coulomb operator everywhere that it appears in the energy calculation:

$$\tilde{Q} = \frac{1}{|\vec{r}_1 - \vec{r}_2|} + \lambda \vec{p}_1 \cdot \vec{p}_2.$$

The operator  $\tilde{Q}$  has the same symmetry and structure as the Coulomb operator. The scaling factor  $\lambda$  is varied, and the energy spectrum is recalculated.  $k_{\text{SMS}}$  is extracted from the numerical derivative

$$k_{\text{SMS}} = \left. \frac{d\omega}{d\lambda} \right|_{\lambda=0}.$$

Values of  $\lambda$  at the level  $10^{-3}$  give a large enough effect while ensuring numerical stability.

Finally, we estimate the values of the field shift parameter,  $F_{\text{FS}}$ , using a finite-field method with a small CI calculation. The field can be a scaled change in the nuclear radius,  $\lambda(U_{R+\delta R} - U_R)$ , where  $U_R$  is the potential of a nucleus with radius  $R$ .  $F_{\text{FS}}$  is then extracted from  $d\omega/d\lambda$  (Berengut et al. 2003). Alternatively, we can simply vary the nuclear radius itself over a larger range and extract  $F_{\text{FS}}$  via  $d\omega/dR$ . Both methods agree. Since the change in potential is a one-body operator and correlations do not strongly affect it, this gives sufficient accuracy in  $F_{\text{FS}}$  for our purposes.

## A1 Silicon

For the silicon calculation we begin with a  $V^{N-1}$  Dirac-Fock calculation, including  $3s^2$  in the core. These orbitals are removed from the core and become valence orbitals for the purposes of both CI and MBPT calculations. This necessitates including subtraction diagrams in the MBPT, but ensures a good starting approximation for the atomic orbitals. An alternative is to use the  $V^{N-3}$  approximation which doesn't include  $3s^2$  in the core; we find that both methods

give consistent results when the CI is saturated and all second-order MBPT diagrams are taken into account.

The CI calculation includes all single and double excitations to the basis set 16spdf from the configurations  $3s^2 3p$ ,  $3s 3p^2$ ,  $3s^2 4p$ , and  $3s^2 3d$ . The MBPT basis is larger, 30spdfg; we tested saturation of the MBPT basis by extending it to 35spdfgh and found that this made no difference to our results. Estimates of the uncertainty in  $k_{\text{SMS}}$  and  $q$  are taken from the difference between full CI+MBPT calculation and the CI alone. Final results are presented in Table A1.

## A2 Titanium

Our titanium calculations follow Berengut et al. (2008) closely. To obtain good starting orbitals in the titanium calculation requires inclusion of  $3d^2$  electrons at the Dirac-Fock level, again corresponding to the  $V^{N-1}$  approximation. To include this, we simply scale the potential due to the filled  $3d^{10}$  level by the factor 2/10, and include it in the Dirac-Fock core. The  $3d$  orbital becomes a valence orbital for the CI and MBPT, and again subtraction diagrams must be included to correct for the change in Dirac-Fock potential.

Saturation at our accuracy is achieved in Ti II with a 16spdf basis in the CI, taking all single and double excitations from the leading configurations  $3d^2 4s$ ,  $3d^2 4p$ ,  $3d 4s 4p$ , and  $3d^3$ . The MBPT diagrams are calculated using the basis 33spdfg. The Ti II spectrum can be further improved by modification of the energy denominator in second-order perturbation theory (Berengut et al. 2008). We add a constant  $\delta$  to the energy denominator:

$$\frac{1}{E - E_M} \rightarrow \frac{1}{E - E_M + \delta}$$

where  $E_M$  is the energy of the intermediate state. By taking  $\delta$  as the difference between the CI and Dirac-Fock energies of the ground state,  $\delta = E^{\text{CI}} - E^{\text{DF}} \approx -0.70$ , we are correcting the ground state energy to the CI value. This shift also restores the correct asymptotic behaviour in the Brillouin-Wigner perturbation theory for a large number of particles (Kozlov & Porsev 1999).

As with our Si II calculation, we estimate uncertainties by taking the difference between the calculations that include MBPT and those that don't. For the  $q$  values we use the difference between the CI and CI+MBPT results that don't include modification of the energy denominator  $\delta$ ; these errors are usually slightly larger and are possibly more indicative of the size of neglected contributions. Final results are presented in Table A2.

A further complication in the calculation of  $q$ -values arises in the Ti II spectrum because of the close proximity of the  $3d 4s 4p \ ^4F^o$  and  $\ ^4D^o$  multiplets, which causes mixing of their  $J = 3/2, 5/2$ , and  $7/2$  levels. Near a level pseudo-crossing, the states become strongly mixed, which can cause the gradient  $d\omega/dx$  to change dramatically. Dzuba et al. (2002) found similar effects in the Fe II spectrum, and used experimental Landé  $g$ -factors to resolve the level of mixing. Since experimental  $g$ -factors are not available for these Ti II lines, we estimate the mixing of the levels from the experimental energy differences and the difference between calculated  $g$ -factors and the  $g$ -factors expected in pure  $LS$ -coupling scheme.

Table A3 shows the result of ‘‘unmixing’’ the levels. For each  $J$ , the difference between the computed value,  $g_{\text{calc}}$ , and the  $LS$  value,  $g_{LS}$ , is used to estimate the amount of mixing of the two levels. With this mixing, it is possible to calculate the  $q$ -values of the unmixed states,  $q_{LS}$ . Our calculation reproduces the experimental  $\ ^4F^o$ – $\ ^4D^o$  energy difference,  $\Delta$ , fairly well, which means our mixing levels are likely to be reasonable. On the other hand, the procedure

**Table A1.** Energy,  $q$ -values and isotope-shift constants for transitions from the Si II ground state  $3s^2 3p^2 P^o_{1/2}$ .

Upper level	J	$\omega_0$ [cm <sup>-1</sup> ]		$k_{\text{NMS}}$ [GHz.amu]	$k_{\text{SMS}}$ [GHz.amu]	$F_{\text{FS}}$ [MHz.fm <sup>-2</sup> ]	$q$ [cm <sup>-1</sup> ]
		Expt.	Theor.				
$3s^2 3p^2 P^o$	3/2	287	304	-5	18 (3)	0	304 (9)
$3s 3p^2^4 P$	1/2	42824	42528	-704	-1577 (97)	-309	470 (17)
	3/2	42933	42644	-706	-1573 (98)	-309	586 (20)
	5/2	43108	42829	-709	-1565 (99)	-309	773 (26)
$3s 3p^2^2 D$	3/2	55309	55233	-910	-1091 (119)	-181	526 (16)
	5/2	55325	55251	-910	-1091 (121)	-181	547 (16)
$3s^2 4s^2 S$	1/2	65500	66067	-1077	1454 (47)	144	47 (4)
$3s 3p^2^2 S$	1/2	76665	76904	-1261	-768 (126)	-279	644 (24)
$3s^2 3d^2 D$	3/2	79339	79588	-1305	1413 (109)	-23	270 (8)
	5/2	79355	79606	-1305	1408 (109)	-24	290 (8)
$3s^2 4p^2 P^o$	1/2	81191	81072	-1335	1085 (53)	90	81 (1)
	3/2	81251	81136	-1336	1088 (54)	90	144 (2)
$3s 3p^2^2 P$	1/2	83802	83912	-1378	462 (134)	-303	544 (17)
	3/2	84004	84127	-1382	476 (133)	-303	756 (23)

**Table A2.** Energy,  $q$ -values and isotope-shift constants for transitions from the Ti II ground state  $3d^2 4s^4 F_{3/2}$ .

Upper level	J	$\omega_0$ [cm <sup>-1</sup> ]		$k_{\text{NMS}}$ [GHz.amu]	$k_{\text{SMS}}$ [GHz.amu]	$F_{\text{FS}}$ [MHz.fm <sup>-2</sup> ]	$q$ [cm <sup>-1</sup> ]
		Expt.	Theor.				
$3d^2 4p^4 G^o$	5/2	29544	29652	-486	-346 (104)	-408	408 (30)
	7/2	29735	29878	-489	-329 (97)	-408	637 (69)
	9/2	29968	30145	-493	-315 (95)	-407	906 (106)
	11/2	30241	30449	-497	-300 (98)	-407	1212 (149)
$3d^2 4p^4 F^o$	3/2	30836	30965	-507	-279 (172)	-411	563 (31)
	5/2	30959	31113	-509	-265 (163)	-411	721 (70)
	7/2	31114	31297	-512	-254 (160)	-411	903 (100)
	9/2	31301	31516	-515	-250 (166)	-410	1119 (129)
$3d^2 4p^2 F^o$	5/2	31207	31431	-513	-248 (193)	-399	657 (47)
	7/2	31491	31769	-518	-224 (178)	-398	988 (110)
$3d^2 4p^2 D^o$	3/2	31757	31992	-522	-194 (244)	-395	655 (98)
	5/2	32025	32311	-527	-188 (243)	-398	956 (173)
$3d^2 4p^4 D^o$	1/2	32532	32755	-535	-225 (224)	-411	739 (79)
	3/2	32603	32853	-536	-228 (236)	-408	855 (84)
	5/2	32698	32976	-538	-225 (245)	-403	999 (62)
	7/2	32767	33063	-539	-215 (225)	-408	1049 (117)
$3d 4s 4p^4 F^o$	3/2	52330	50831	-861	3656 (510)	346	-1689 (250)
	5/2	52472	51000	-863	3671 (512)	347	-1482 (370)
	7/2	52705	51264	-867	3692 (509)	348	-1198 (360)
	9/2	53099	51656	-873	3702 (517)	349	-910 (193)
$3d 4s 4p^4 D^o$	1/2	52339	50870	-861	3712 (584)	330	-1414 (166)
	3/2	52459	50977	-863	3692 (601)	330	-1343 (250)
	5/2	52631	51155	-866	3686 (614)	330	-1209 (370)
$3d 4s 4p^2 D^o$	7/2	52847	51401	-869	3708 (614)	332	-992 (360)
	5/2	53555	52392	-881	3263 (603)	235	-882 (182)
	3/2	53597	52449	-881	3264 (607)	236	-819 (191)

to derive  $q_{LS}$  is sensitive to small changes in  $g_{\text{calc}}$ , and this could artificially exaggerate the differences between the  $q_{LS}$  found for the different levels, particularly for the strongly mixed  $J = 5/2$  and  $J = 7/2$  cases.

Therefore in Table A2 we present the calculated  $q$ -values,  $q_{\text{calc}}$ , and simply increase the errors to account for all possible mixing coefficients. At worst, this will overestimate our uncertainties. Better  $q$ -values will be possible when the experimental  $g$ -factors for these levels are determined. Finally, we note that this mixing doesn't affect the specific mass shift calculations simply because the  $3d 4s 4p^4 F^o$  and  $4D^o$  levels have very similar  $k_{\text{SMS}}$  values anyway.

## SUPPORTING INFORMATION

Additional Supporting Information may be found in the online version of this article:

**Atomic Data spreadsheet.** Comprehensive record of the measurements and theoretical estimates from the literature, plus the calculations performed in this paper, which contribute to the synthesized information presented in Tables 2–11 (*Oxford University Press to supply URL*). An up-to-date version of the spreadsheet is maintained by M.T.M. and is available through <https://researchdata.ands.org.au/laboratory-atomic-transition-data-for-precise-optical-quasar-absorption-spectroscopy>. The authors welcome updated information for inclusion in new versions.

**Table A3.** Mixing of the  $3d4s4p\ ^4F^o$  and  $^4D^o$  multiplets in Ti II. The difference between the calculated and  $LS$   $g$ -factors is used to estimate the proportion of mixing at  $\alpha = \alpha_0$ .  $\Delta$  is the energy difference between the two levels for each angular momentum,  $J$ .  $q_{\text{calc}}$  is the computed  $q$ -value, while  $q_{LS}$  is the expected  $q$ -value in the absence of the level pseudocrossing.

	$g_{LS}$	$g_{\text{calc}}$	Mixing	$\Delta$ [ $\text{cm}^{-1}$ ]		$q_{\text{calc}}$	$q_{LS}$
				expt.	calc.	[ $\text{cm}^{-1}$ ]	[ $\text{cm}^{-1}$ ]
$J = 3/2:$							
$^4F^o$	0.400	0.533	16%	129	147	-1689	-1774
$^4D^o$	1.200	1.071				-1343	-1259
$J = 5/2:$							
$^4F^o$	1.029	1.137	32%	159	156	-1482	-1719
$^4D^o$	1.371	1.263				-1209	-973
$J = 7/2:$							
$^4F^o$	1.238	1.306	36%	141	137	-1198	-1457
$^4D^o$	1.429	1.360				-992	-732

Please note: Oxford University Press are not responsible for the content or functionality of any supporting materials supplied by the authors. Any queries (other than missing material) should be directed to the corresponding author for the article

This paper has been typeset from a  $\text{\TeX}/\text{\LaTeX}$  file prepared by the author.